AD-A163 309 ASPECTS OF THE CALCULATION OF BOUNDARY LAYERS ON SHIPS' 1/2
(U) SCIENCE APPLICATIONS INTERNATIONAL CORP ANNAPOLIS
MD C H VON KERCZEK DEC 85 SAIC-85/1158
UNCLASSIFIED N00014-82-C-0599 F/G 20/4 NL

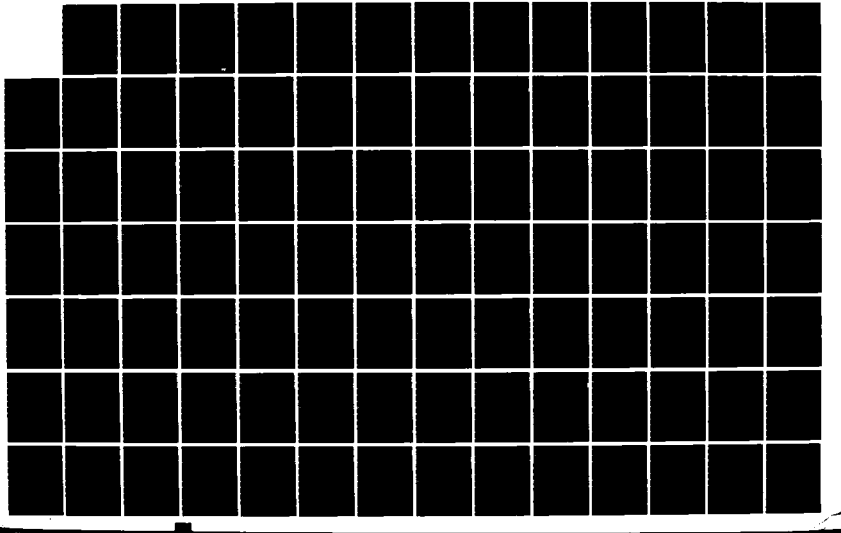

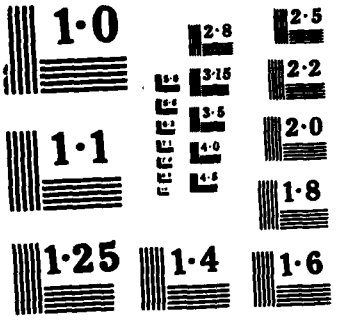

NATIONAL BUREAU OF STANDARDS
MICROCOPY RESOLUTION TEST CHART

(2)

ASPECTS OF THE CALCULATION OF BOUNDARY LAYERS ON SHIPS' PROPELLERS

(FINAL REPORT)

SAIC-85/1158

Science Applications International Corporation

ASPECTS OF THE CALCULATION OF BOUNDARY LAYERS ON SHIPS' PROPELLERS

(FINAL REPORT)

SAIC-85/1158

December 1985

Prepared by

Christian H. von Kerczek
SAIC/Annapolis

Prepared for

Office of Naval Research
800 N. Quincy Street
Arlington, Virginia 22217

ONR Contract N00014-82-C-0599

SCIENCE APPLICATIONS INTERNATIONAL CORPORATION

134 Holiday Court, Suite 318
Annapolis, Maryland 21401
(301) 266-0091, D.C.: 261-8026

UNCLASSIFIED

SECURITY CLASSIFICATION OF THIS PAGE (When Data Entered)

REPORT DOCUMENTATION PAGE		READ INSTRUCTIONS BEFORE COMPLETING FORM
1. REPORT NUMBER SAIC-85/1158	2. GOVT ACCESSION NO.	3. RECIPIENT'S CATALOG NUMBER
4. TITLE (and Subtitle) ASPECTS OF THE CALCULATION OF BOUNDARY LAYERS ON SHIPS' PROPELLERS		5. TYPE OF REPORT & PERIOD COVERED Technical Report 07/15/84 - 10/14/85
		6. PERFORMING ORG. REPORT NUMBER
7. AUTHOR(s) Christian H. von Kerczek		8. CONTRACT OR GRANT NUMBER(s) N00014-82-C-0599
9. PERFORMING ORGANIZATION NAME AND ADDRESS Science Applications International Corp. 134 Holiday Court, Suite 318 Annapolis, Maryland 21401		10. PROGRAM ELEMENT, PROJECT, TASK AREA & WORK UNIT NUMBERS
11. CONTROLLING OFFICE NAME AND ADDRESS Office of Naval Research 800 N. Quincy Street Arlington, Virginia 22217		12. REPORT DATE December 1985
		13. NUMBER OF PAGES
14. MONITORING AGENCY NAME & ADDRESS(if different from Controlling Office)		15. SECURITY CLASS. (of this report) UNCLASSIFIED
		15a. DECLASSIFICATION/DOWNGRADING SCHEDULE

16. DISTRIBUTION STATEMENT (of this Report)

UNLIMITED

17. DISTRIBUTION STATEMENT (of the abstract entered in Block 20, if different from Report)

UNLIMITED

18. SUPPLEMENTARY NOTES

19. KEY WORDS (Continue on reverse side if necessary and identify by block number)

Boundary Layers, Laminar, Three-Dimensional

20. ABSTRACT (Continue on reverse side if necessary and identify by block number)

Some aspects of three-dimensional laminar boundary layers at attachment lines were investigated. In particular, the boundary layer on the attachment line between a nodal and saddle point of attachment was solved by numerical and perturbation methods. It was shown that the boundary layer equations could be solved in the separated region near the saddle point without viscous/inviscid interactions. The general three-dimensional boundary

DD FORM 1 JAN 73 1473 EDITION OF 1 NOV 65 IS OBSOLETE

S/N 0102-LF-014-6601

UNCLASSIFIED

SECURITY CLASSIFICATION OF THIS PAGE When Data Ente...

layer on oblate spheroids in edgewise flow was also investigated. Attention was focussed on crossflow reversal near the lateral ends (tips) of the spheroid.

TABLE OF CONTENTS

TABLE OF CONTENTS (continued)

ASPECTS OF THE CALCULATION OF BOUNDARY LAYERS ON SHIPS' PROPELLERS (FINAL REPORT)

EXECUTIVE SUMMARY

The calculation of the boundary layer on marine propellers is important for several reasons. Viscous losses in propeller performance can be determined by such a computational capability. However, the determination of the detailed viscous flow in the propeller root and tip regions is even more important because the flow in these regions directly affects the hub and tip vortex generation process. These vortices play an important role in propeller noise, cavitation and overall performance. Furthermore, the laminar boundary layer at the leading edge of model propellers plays a very important role in the correlation of the cavitation performance of model to full scale propellers.

Computational methods for calculating the boundary layer on the faces of a propeller blade have been developed by Groves (1981) and Groves and Chang (1985). These methods ignore or only crudely approximate the flow at the root and leading edge of the propeller. The leading edge flow has a profound effect on the tip flow when the blades are swept back as on highly skewed propellers.

This study focussed on those aspects of the propeller problem that have not been treated satisfactorily by Groves and Chang. In particular the leading edge boundary layer was the main object of study. However, in the course of this study another important aspect of leading edge boundary layers emerged that has considerably wider application than marine propellers. This aspect concerns the way boundary layers emerge from points of attachment and the flow along the attachment line connecting multiple points of attachment. These aspects will be clarified below. At present it need only be noted that these attachment line problems occur also at the bow of destroyer hulls with a protruding sonar bulb and also at wing (or foil)/body intersections if the wing is at least slightly swept foreward. Also, the flow along such an attachment line is an interesting model problem that may have important implications to the horseshoe vortex rollup at the leading edge of a wing body intersection.

This report is divided into two main parts describing the research performed under this contract. The first part describes the work concerning the flow on the attachment line connecting a nodal and saddle point of attachment. The second part describes the work concerning the flow near a leading edge of a wing or blade.

The research performed in the first part, concerning the flow between nodal and saddle points of attachment had a very interesting outcome. One of the main findings is that there can exist separation along the attachment line that manifests itself as a horseshoe vortex perpendicular to the attachment line and wraps around the body. Under certain circumstances this horseshoe vortex is embedded in the boundary layer and the separated flow does not disturb the external potential flow. Thus this flow can be calculated by ordinary boundary layer theory without viscous/inviscid interactions. The various aspects of this work described in the report will be abridged and submitted to technical journals. One paper has already been submitted.

The second part of this research concerning the leading edge flow on blades or wings has not been as successful. A model problem consisting of a very flat oblate spheriod (say a disk) in an edgewise stream was examined. The boundary layer could be calculated when the disk was at zero angle of attack. However, great difficulty was encountered in developing a stable method that would properly account for the flow in the vicinity of the curved dividing streamline that separates the flow going over the top and bottom of the disk. At an angle of attack this dividing streamline is no longer the edge symmetry plane, but it curls

off the edge to the windward (pressure) side of the disk. A full description of the work and results of this effort is given in the report. We give below a summary of the status of the propeller leading edge problem:

(i) A numerical method for dealing with the 3D laminar boundary layer equations, with rotation, and in non-orthogonal surface coordinates has been developed and programmed.

(ii) The method has been set up in a general way so that a variety of coordinate sytems can be handled easily as demonstrated in Sections 4 and 5 of Part II of this report.

(iii) The method can deal successfully with non flat bodies such as ship bows and elongated bodies at zero or nonzero angles of attack, such as ovary spheroids or, more practically, submarines or torpedoes. In fact, the same basic set of algorithms and codes were used for the direct numerical integration of the attachment line boundary layer of Part I. This type of calculation has direct relevance to destroyer bows.

(iv) A new method for advancing from the stagnation point along the foreward curve of attachment near a leading edge of a flattened body such as a wing or blade was unsuccessful. The method does not seem to have any flaws and at this time it is not certain whether coding errors have prevented success in using this method.

(v) Some alternative methods to achieve success in calculating the leading edge flow might be to use an explicit backward differencing with respect to the crossflow coordinate or to apply the characteristic box method. Resources of the present contract have not permitted us to embark on efforts to develop these alternative methods.* It is believed, that a modest further effort can resolve the problem at the attachment line and result in a very useful, and versatile three-dimensional boundary layer code.

---

* At this stage only our inability to handle the starting conditions at a general attachment line prevents our code from being a complete general 3D laminar boundary layer program.

REFERENCES

Groves, N.C. (1981), "An integral prediction method for three-dimensional turbulent boundary layers on rotating blades," Propellers '81, Soc. Nav. Arch. Marine Eng., New York.

Groves, N.C. and Chang, M.S. (1985), "A differential prediction method for three-dimensional laminar and turbulent boundary layers of rotating propeller blades," DTNSRDC Report 85/058.

Appendix B

(Paper submitted to ASME J. Appl. Mech.)

Boundary Layer Separation Between Nodal and Saddle points of Attachment

by

C. H. von Kerczek

1. Introduction

The inviscid surface velocity at a stagnation point of attachment $(x,y)=(0,0)=P$ can be described by $U=ax$ and $V=by$ with $b>0$ in the orthogonal coordinates x and y respectively. The stagnation point of attachment P is characterized by the value of $c=a/b$. For the values of $c>$ or $=0$ the point P is a nodal point. The stagnation point boundary layer at a nodal point was completely solved by Howarth (1951). For the values of $c<0$ the point P is a saddle point. The boundary layer at a saddle point was solved by Davey(1961). Davey showed that for values of $c<-1.0$ no boundary layer solutions exist that meet the outer boundary conditions imposed by the above inviscid flow. He also showed that for values of $c<-0.4294$ the flow in the x direction develops a reversed flow at the wall, ie., the boundary layer separates. However, the separated flow exists as a solution of the stagnation point boundary layer equations for all values of c in the range $-1.0<c<-0.4294$.

The following question arizes: Are the saddle point solutions affected by the flow along the symmetry plane ($y=0$) that emanates from the nodal point? Or, is the saddle point flow so dominant that no matter how the flow begins upstream at the nodal point, the solution always evolves into Davey's saddle point solution. Cooke and Robins (1970) investigated this question by numerically integrating

the symmetry plane boundary layer equations from the nodal point to the saddle point. They did this in two ways. The first way was by series expansions about the nodal and saddle point. These series were found to overlap and thus allowed the calculation of the boundary layer between the two points of attachment. The second way they calculated the symmetry plane boundary layer was by direct numerical integration.

Cooke and Robins carried out these calculations only for values of c>or=-0.4294 so that the boundary layer did not separate along the attachment line. Only for the case c=-0.4294 did the boundary layer separate at the saddle point, just as Davey predicted it would. Thus Cooke and Robins showed that for values of c>or=-0.4294 Davey's saddle point solution always emerges as the natural termination of a flow from the nodal point to the saddle point. The question still remains if the separated solutions will emerge as the natural termination of the flow along the x-axis. In particular, if the flow at the saddle point is separated then there must be a separation point on the x-axis ahead of the saddle point. Can the boundary layer flow proceed through this separation point towards the saddle point without altering the external inviscid flow? It would seem that this must happen because Davey's saddle point solutions exist for the given inviscid flow. Furthermore, Klemp and Acrivos (1976) have shown that there do exist boundary layers with separation that do not disturb the external potential flow.

This note presents some calculations that show the attachment line boundary layer between a nodal and saddle point for some values of c<-0.4294 for which the boundary layer along the x-axis separates ahead of the saddle point. Nevertheless, the saddle point is reached

with Davey's separated velocity profile. It should be mentioned that this attachment line boundary layer finds practical application to the flow along the stem of bulbous bowed ships.

2. Formulation of the Attachment Line Flow

Cooke and Robins considered the model flow over a plane surface z=0 on which the inviscid velocity (U,V,W) is given by

$$U=ax(1-x)+az^2, \quad V=by, \quad W=-(a+b-2ax)z. \tag{1}$$

The z-axis is perpendicular to the surface. The nodal point of attachment is the point (0,0,0) and the saddle point is (1,0,0). The line of attachment is y=0, z=0. The boundary layer flow velocity (u',v',w') in the (x,y,z) directions respectively is rescaled as follows:

$$u'=Uu(x,z'), \quad v'=Vv(x,z'), \quad w'=(b/Re)^{1/2}w(x,z') \tag{2}$$

where $z'=(bRe)^{1/2}z$ and Re is the Reynolds number. The resulting y=0 symmetry plane boundary layer equations are

$$w_{z'}+ex(1-x)u_x+e(1-2x)u+v=0, \tag{3}$$

$$u_{z'z'}-wu_{z'}-e(1-2x)u^2-ex(1-x)uu_x=-e(1-2x), \tag{4}$$

$$v_{z'z'}-wv_{z'}-v^2-ex(1-x)uv_x=-1. \tag{5}$$

Equation (3) is the continuity equation and (4) and (5) are

the x and y momentum equations respectively. The parameter e=a/b, b>0. For e>0 the nodal point is at x=0 and the saddle point is at x=1. Thus at the saddle point x=1 e is the same as -c. For negative values of e x=0 is the saddle point and x=1 is the nodal point. For e>0 the flow along the x-axis is from x=0 to x=1 and the v-component of the flow is always away from the x-axis. The equations (3-5) are quasi two-dimensional and are solved subject to the boundary conditions

$$u=v=w=0 \text{ at } z'=0 \quad \text{and} \quad u=v=1 \text{ at } z'=\text{infinity}. \tag{6}$$

These equations were solved numerically using the well known Keller box method (see Cebeci and Bradshaw,1977). In the region of flow separation the numerical integration was continued in the forward direction (x>0) by employing the FLARE approximation. This approximation sets u=0 whenever u<0 and u occurs as a coefficient of u_x.

3. Results and Discussion

The results of the numerical solution of equations (3-6) are shown in Figure 1. There the wall skin friction coefficient $Cf_x = (bRe)^{1/2}U(du/dz')_o$ is plotted versus x for three values of e. The case e=0.25 corresponds to no separation of the flow in the x-direction. This case was presented by Cooke and Robins and the present results are virtually identical to theirs. In the second and third cases of e=0.5 and 0.6 the u component of the boundary layer separates ahead (x<1) of the saddle point of attachment. However the numerical integration method was able to proceed through the separated flow region to the saddle point. For values of e slightly larger than 0.6 the marching method breaks down before the saddle

point is reached. The values of Cf_x/U predicted by the numerical integration at the saddle point x=1 are -0.1115 and -0.2668 for e=0.5 and 0.6 respectively. These values of Cf_x/U are in very good agreement with Davey's results. They show that even in the case of separated flow Davey's saddle point solutions emerge from the flow towards the saddle point, albeit for values of e only slightly larger than 0.4294.

The question remains wether flow separation along the attachment line y=0 can occur without disrupting the external inviscid flow for larger values of e. Although the present numerical integration method using the FLARE approximation failed to yield solutions all the way to the saddle point for values of e>0.6 this is not conclusive evidence that such solutions with the given inviscid flow are not possible. Davey speculates that once separation does occur on the attachment line the boundary layer flow interacts with the external inviscid flow in such a way that the saddle point becomes a nodal point of attachment. This certainly must occur for e>1, but not necessarily for e<1. In order to verify if separated solutions with the inviscid flow (1) are possible for values of e>0.6 a more robust method for solving these boundary layer equations is needed. The method of Klemp and Acrivos (1976) seems to be a possibility. They treated a problem in which the boundary layer containes an imbedded separated region but the external inviscid flow was unaffected by this separation. Another method that is presently being persued is the use of high order series expansions in terms of the parameter e. The point of expansion is the two-dimensional stagnation line solution given by e=0.

4. References

Cebeci,T and Bradshaw,P. (1977) Momentum Transfer in Boundary Layers, McGraw-Hill, New York.

Cooke,J.C. and Robins,A.J. (1970) J. Fluid Mech., 41, 823.

Davey,A. (1961) J. Fluid Mech., 10, 593.

Howarth,L. (1951) Phil. Mag.(7), 42, 1433.

Klemp,J.B. and Acrivos,A. (1976) J. Fluid Mech., 76, 363.

Acknowledgement: This research was sponsored by the ONR under contract N00014-82-C-0599.

Figure Caption:

Fig.1 Plot of Cf_x vs x for values of e=0.25,0.5 and 0.6. The nodal point is at x=0 and the saddle point is at x=1.

Part I

THE BOUNDARY LAYER ALONG THE ATTACHMENT LINE BETWEEN A NODAL AND SADDLE POINT OF ATTACHMENT

Section 1

INTRODUCTION

Consider the viscous flow around a corrugated circular cylinder as shown in Figure 1. The approaching flow is perpendicular to the axis of the cylinder. Let the curve marked by the points labeled N and S be the intersection of the cylinder with the meridian plane containing the cylinder axis and the oncoming stream velocity vector. Let e be a measure of the amplitude of the corrugations.

The curve containing the points N and S is the attachment line of the flow and the points N and S are the nodal and saddle points of attachment respectively. The points N and S are stagnation points of the external inviscid flow. At the attachment line the flow divides and proceeds around the circumference of the cylinder. In the case of a straight cylinder, e=0, the attachment line is entirely one of stagnation. It is then the classical 2D stagnation line found in all planar flows about cylindrical bodies. In the case of the corrugated cylinder there is a spanwise flow along the attachment line. This spanwise flow emanates from the nodal point and terminates at the saddle point. A three dimensional boundary layer calculation around the corrugated cylinder must begin with the calculation of

the attachment line flow. This is analogous to the calculation of the symmetry plane boundary layer in ordinary three dimensional boundary layers.

This corrrugated cylinder boundary layer is being considered because it is a model problem for several important practical boundary layer problems. The most important of these practical problems is the flow at the bow of a sonar domed destroyer hull as shown schematically in Figure 2. Boundary layer calculation methods must start at stagnation points and lines of attachment. Up to the present time all calculation methods have only dealt with simple nodal points of attachment in general three dimensional flows. Thus these methods cannot deal properly with flow around bulbous bowed destroyers. Indeed, practical ship boundary layer calculation methods deal with turbulent flows that begin downstream of the front stagnation point. The calculation methods are started with artifical initial data (or experimental data when available, see Groves, 1981). However, on bow geometries as the one depicted in Figure 2 the boundary layer emanating from the attachment line between the nodal and saddle point can separate to form a horseshoe vortex wrapped around the stem of the ship and trailing downstream along the sides. Thus, ignoring the bow flow would result in missing this very important aspect of the boundary layer.

It is also fairly obvious that if the parameter e characterizing the corrugation amplitude becomes large the geometry will have a certain crude resemblance to a filleted hull/appendage intersection. This type of intersection problem is very important in many flow configurations. In the present study it was, in fact, the hub/blade intersection that led us to consider the corrugated cylinder problem.

In this study only the flow along the attachment line between points N and S was considered. This flow serves as the starting point of a complete calculation of the flow around the cylinder. In the overall flow field the attachment line flow serves as the initial conditions for the cross-flow. The mainstream flow is around the circumference perpendicular to the attachment line.

The external inviscid flow driving the attachment line flow and the governing laminar boundary layer equations are given in Section 2. Section 3 describes the flow directly at the saddle point of attachment. This flow can be considered in isolation. Indeed, Davey (1961) solved the saddle point flow completely, but left many unanswered questions concerning the relationship of the saddle point flow to the rest of the attachmment line flow. This flow has been reconsidered here using a different kind of numerical

method in order to set the stage for the calculation of the attachment line flow. Section 4 details the results and limitations of a straightforward numerical integration of the attachment line flow. Section 5 presents a high order perturbation method to calculate the attachment line flow and the results obtained by this method. The last section, Section 6, gives some closing remarks concerning methods for solving the attachment line flow on practical configurations and extension to turbulent flows.

Section 2

FORMULATION OF THE ATTACHMENT LINE FLOW

Let the surface arclength coordinate along the attachment line be denoted by x and let y be the coordinate normal to x and tangent to the surface of the cylinder. Let z be the coordinate normal to the cylinder surface. Then in the vicinity of the attachment line the potential flow on the surface of the cylinder has the velocity distribution $\vec{V}$ given by

$$\vec{V} = e \sin x \, \vec{i} + y \, \vec{j} \, . \tag{1}$$

The surface velocity field $\vec{V}$ given by equation (1) is obtained by considering small amplitude corrugations and calculating the small deviations of the resulting flow from the flow around a straight circular cylinder (see Davey, 1961). There are an infinite number of nodal points at $x=2n\pi x$ and an infinite number of saddle points at $x=(2n+1)\pi x/2$ for $n=0,\pm1,\pm2,\ldots$ Only the node at $x=0$ and the saddle at $x=\pi$ is considered in this study. The rest of the nodes and saddles are the same as $x=0$ and π respectively by symmetry.

The three dimensional boundary layer equations in general orthogonal coordinates are the following (see Rosenhead, 1963): The continuity equation is

$$\frac{\partial u}{\partial x} + \frac{\partial v}{\partial y} + \frac{\partial w}{\partial z} + K_1 u + K_2 v = 0 \tag{2}$$

The momentum equation along the attachment line x is

$$u\frac{\partial u}{\partial x} + v\frac{\partial u}{\partial y} + w\frac{\partial u}{\partial z} + K_1 uv - K_2 v^2 = -\frac{\partial p}{\partial x} + \nu\frac{\partial^2 u}{\partial z^2} \tag{3}$$

The momentum equation in the y direction is

$$u\frac{\partial v}{\partial x} + v\frac{\partial v}{\partial y} + w\frac{\partial v}{\partial z} + K_2 uv - k_1 u^2 = -\frac{\partial p}{\partial y} + \nu\frac{\partial^2 v}{\partial z^2} \tag{4}$$

The boundary layer velocity is denoted by (u,v,w) in the (x,y,z) directions respectively. The pressure is denoted by p and can be computed by Bernoulli's equation as

$$p_o - p = (1/2)\rho \vec{v} \cdot \vec{v} \tag{5}$$

It is assumed here that x, y and z are arclength coordinates so that the metric coefficients can be suppressed.

The quantities K_1 and K_2 are the geodesic curvatures of the x=constant and y=constant curves respectively. The attachment line is a symmetry line so the K_2=0. The geodesic curvature K_1=(1/r)dr/dx, where r=r(x) is the local radius of the cylinder. However, K_1 is neglected in this study simply because it plays a negligible qualitative role. The term can be easily included, but in this model problem only the main pressure distribution is of interest.

The boundary conditions on u, v and w are the following:

$$u = v = w = 0 \qquad \text{at } z=0 , \tag{6}$$

$$u = e \sin x , \; v=y \quad \text{at } z \to \infty . \tag{7}$$

The boundary layer velocity field (u,v,w) is rescaled as

$$u = e \sin xf , \; v = yh , \; w = \sqrt{\nu}\, g \tag{8}$$

and the vertical coordinate z' is defined as

$$z = \sqrt{\nu}\, z' . \tag{9}$$

Furthermore, the velocity gradients q and r are defined as

$$\frac{\partial f}{\partial z'} + q = 0 \tag{10}$$

$$\frac{\partial h}{\partial z'} + r = 0 \tag{11}$$

Then equations (2), (3), (4), (10) and (11) can be rewritten as (in the order of 11, 2, 4, 10, 3 respectively)

$$\frac{\partial h}{\partial z} + r = 0 \tag{12}$$

$$\text{esinx } \frac{\partial f}{\partial x} + \frac{\partial g}{\partial z} + \text{ecosx} f + h = 0 \tag{13}$$

$$\text{esinx } f \frac{\partial h}{\partial x} + \frac{\partial r}{\partial z} - gr + h^2 = 1 \tag{14}$$

$$\frac{\partial f}{\partial z} + q = 0 \tag{15}$$

$$\text{esinx } f \frac{\partial f}{\partial x} + \frac{\partial q}{\partial z} - gq + \text{ecosx } f^2 = \text{ecosx} \tag{16}$$

with the prime on z dropped and the new boundary conditions

$$f = h = g = 0 \qquad \text{at } z=0 \tag{17}$$

and

$$f = h = 1 \qquad \text{at } z \to \infty \ . \tag{18}$$

These boundary layer equations (12 - 18) can be solved by marching from the nodal point x=0 to the saddle point $x=\pi$. Note that the inviscid flow vanishes at the saddle point and that the u component of velocity points into the saddle point, much like a rear stagnation point. It is well known (see Rosenhead, 1963) that the boundary layer equations have no solutions at a nodal point of separation. But a saddle point differs from a nodal point of separation in that the velocity in one direction flows away from the stagnation point. This outflow is so strong that the vertical flow at the stagnation point is downward rather than upward. For example, the inviscid flow Eq. (1) has the form

$$\vec{V} = e \sin x \, \vec{i} + y \, \vec{j} - z \, (1+e\cos x) \, \vec{k} \tag{19}$$

for small values of z just above the surface. At the saddle point $x=\pi$ the $\vec{k}$ component of velocity is towards the body as long as $e<1$ and thus the boundary layer vorticity is not transported away from the wall. Once $e>1$ the k component of velocity is away from the wall and the saddle point behaves like a nodal point of separation (i.e., a rear stagnation

point on a closed body) at which steady boundary layer solutions do not exist.

It is also interesting to note that the parameter e characterizes the local geometry at the nodal and saddle points. For example, at the nodal point x=0, e=1 corresponds to a spherical stagnation point for which the curvature is the same in every direction. The value e=0 is the two dimensional stagnation line. This knowledge suggests an alternative way of dealing with equations (12 - 18). This alternative is to calculate the boundary layer as an asymptotic expansion in e about e=0. This is indeed one of the techniques used in the present study and will be described in a later section.

As a preliminary analysis of the full attachment line problem, Eqs.(12 - 18), the special case of the saddle point flow $x=\pi$ will be examined by a perturbation expansion about e=0 in the next section.

Section 3

THE SADDLE POINT FLOW

3.1 BASIC EQUATIONS

The flow at the saddle point of attachment, $x=\pi$ in Eqs. (12 - 18), is governed by the following eqs.

$$\frac{\partial h}{\partial z} + r = 0 \tag{20}$$

$$\frac{\partial g}{\partial z} + h = ef \tag{21}$$

$$\frac{\partial r}{\partial z} - gr + h^2 = 1 \tag{22}$$

$$\frac{\partial f}{\partial z} + q = 0 \tag{23}$$

$$\frac{\partial q}{\partial z} - gq - ef^2 = - e \tag{24}$$

with the boundary conditions

$$f = g = h = 0 \qquad \text{at } z=0 \tag{25}$$

and

$$f = h = 1 \qquad \text{at } z=\infty \ . \tag{26}$$

In fact these equations also govern the flow at the nodal point for values of $-1 \leq e \leq 0$. Davey (1961) solved these equations numerically for values of $0 \leq e \leq 1$. He found that for values of $e \geq 0.4294$ the flow at the saddle point shows a separated u (f) component velocity profile. This indicates that the attachment line flow will separate ahead of the saddle point for values of e in the range $0.4294 < e < 1$. This separation is what initiates the horseshoe vortex that will wrap around the necked down region of the corrugated cylinder. However, Davey does not make any calculations on the attachmment line.

In the present study the attachment line equations will be solved by direct numerical integration and by small e-expansions. For this reason it is worthwhile to consider the simpler case of the small e-expansion at the saddle point to check the results with Davey's solutions. Furthermore, this small e-expansion at the saddle point will indicate the range of validity, for a given number of terms, of the general case.

The vector $(h,g,r,f,q)^+ = \vec{F}$ is expanded in e as follows:

$$\vec{F} = \sum_{n=0}^{\infty} e^n \vec{F}_n \tag{27}$$

where

$$\vec{F}_n = \vec{F}_n(z) = (h_n, g_n, r_n, f_n, q_n)^+ .$$

By substituting $\vec{F}_n$ into equations (20 - 26) and grouping terms according to their power of e, the following sequence of perturbation equations result.

O(1):

$$\left.\begin{aligned} \frac{\partial h_o}{\partial z} + r_o &= 0 \\ \frac{\partial g_o}{\partial z} + h_o &= 0 \\ \frac{\partial r_o}{\partial z} - g_o r_o + h_o^2 &= 1 \end{aligned}\right\} \tag{28a,b,c}$$

$$\left.\begin{aligned} \frac{\partial f_o}{\partial z} + q_o &= 0 \\ \frac{\partial q_o}{\partial z} - g_o q_o &= 0 \end{aligned}\right\} \tag{28d,e}$$

with boundary conditions

$$f_o = h_o = g_o = 0 \qquad \text{at } z=0$$

$$f_o = h_o = 1 \qquad \text{at } z=\infty \ . \qquad \text{(28f,g)}$$

O(e):

$$\left.\begin{aligned} &\frac{\partial h_1}{\partial z} + r_1 = 0 \\ &\frac{\partial g_1}{\partial z} + h_1 = f_o \\ &\frac{\partial r_1}{\partial z} - (g_o r_1 + r_o g_1 - 2h_o h_1) = 0 \end{aligned}\right\} \qquad \text{(29a,b,c)}$$

$$\left.\begin{aligned} &\frac{\partial f_1}{\partial z} + q_1 = 0 \\ &\frac{\partial q_1}{\partial z} - (g_o q_1 + q_o g_1) = f_o^2 - 1 \end{aligned}\right\} \qquad \text{(29d,e)}$$

with boundary conditions

$$f_1 = h_1 = g_1 = 0 \qquad \text{at } z=0$$

$$f_1 = h_1 = 0 \qquad \text{at } z=\infty . \qquad \text{(29f,g)}$$

In the general case of $O(e^n)$ for $n \geq 2$ the equations are

$$\left.\begin{aligned} &\frac{\partial h_n}{\partial z} + r_n = 0 \\ &\frac{\partial g_n}{\partial z} + h_n = f_{n-1} \\ &\frac{\partial r_n}{\partial z} - (g_o r_n + r_o g_n - 2h_o h_n) = \sum_{j=1}^{n-1} (g_j r_{n-j} - h_j h_{n-j}) \end{aligned}\right\} \quad (30a,b,c)$$

$$\left.\begin{aligned} &\frac{\partial f_n}{\partial z} + q_n = 0 \\ &\frac{\partial q_n}{\partial z} - g_o q_n = \sum_{j=1}^{n} g_j q_{n-j} \end{aligned}\right\} \quad (30d,e)$$

with boundary conditions

$$\begin{aligned} &f_n = h_n = g_n = 0 \qquad \text{at } z=o \\ &f_n = h_n = 0 \qquad \text{at } z=\infty . \end{aligned} \quad (30f,g)$$

At order 1 the equations (28a,b,c) are simply the planar stagnation point equations. It is interesting to note that in this case the equations (28d,e) are exactly the same

as the temperature equation with Prandtl number equal to one at a planar stagnation point. If the function $g_o(z)$ is known then attachment line flow (f_o,q_o) (and all the f_n,q_n's for that matter) can be found by quadratures. This will be very useful in the subsequent analysis.

3.2 NUMERICAL METHOD

The problems (28) - (30) can be solved sequentially by numerical methods. It is desirable to calculate as many terms as possible of this perturbation series. If a sufficient number of terms of sufficiently high accuracy can be obtained then it may be possible, even for a limited radius of convergence, to obtain values of the flow velocities over the entire range of values of e. Thus, the numerical method for solving the differential equations in problems (28) - (30) needs to be as accurate and efficient as possible. The following numerical method, based on Hermite interpolation, is used. This method will be called the "Hermite box" method.

The equations (28a,b,c) - (30a,,b,c) all reduce to the form

$$\frac{d\vec{F}}{dz} = \vec{F}' = A\cdot\vec{F} + \vec{b} \qquad (31)$$

where the n subscript on $\vec{F}$ has been suppressed. The matrix A can be a function of $\vec{F}$ and thus the equations are nonlinear. However, these equations can be quasi-linearized in a simple form such as replacing $A(\vec{F})$ by $A(\vec{F}_*)$ where $\vec{F}_*$ is the value of $\vec{F}$ at a prior iteration step. Then an iterative procedure of solving (31) with $A(\vec{F}_*)$ will converge to the desired solution $\vec{F}$. It should be noted that only the equations (28a,b,c) are nonlinear. Once these have been solved then the rest of the equations are linear and the coefficient matrices only depend on $\vec{F}_o$. Thus only the equations (28a,b,c) need to be quasi-linearized and iterated to convergence. It is presumed from here on that this is done.

By Hermite interpolation it can be shown that equations (31) can be numerically solved on a partition $\{z_i\}$ of the z interval $(0,z_\infty)$ where $z_\infty >> 1$ but $z_\infty < \infty$, by any of the following sequence of finite difference methods:

$$\vec{F}_i = \vec{F}_{i-1} + \frac{\Delta z_i}{2}(\vec{F}_i' + \vec{F}_{i-1}) + \frac{\Delta z_i^3}{12}\vec{F}''(\xi) \qquad (32)$$

$$\vec{F}_i = \vec{F}_{i-1} + \frac{\Delta z_i}{2}(\vec{F}_i' + \vec{F}_{i-1}') + \frac{\Delta z_i^2}{12}(-\vec{F}_i'' + \vec{F}_{i-1}'') + \frac{\Delta z_i^5}{720}\vec{F}^{(5)}(\xi) \qquad (33)$$

$$\vec{F}_i = \vec{F}_{i-1} + \frac{\Delta z_i}{2}(\vec{F}_i' + \vec{F}_{i-1}') + \frac{\Delta z_i^2}{10}(-\vec{F}_i'' + \vec{F}_{i-1}'')$$

$$+ \frac{\Delta z_i^3}{120}(\vec{F}_i''' + \vec{F}_{i-1}''') + \frac{\Delta z_i^7}{100800}\vec{F}^{(7)}(\xi) \quad (34)$$

etc. for even higher orders. In these formulas primes and superscripts in parenthesis indicate differentiation with respect to z.

The derivatives of $\vec{F}$ can be obtained exactly by using the original differential equation (32). For example,

$$\vec{F}'' = (A\cdot\vec{F}+\vec{b})' = A' \cdot \vec{F} + A \cdot (A\cdot\vec{F}+\vec{b}) + \vec{b}'$$

so that

$$\vec{F}'' = (A^2+A') \cdot \vec{F} + \vec{b}' + \vec{b} .$$

The higher derivatives are obtained in an analogous manner. The resulting system of algebraic equations depend only on powers and derivatives of the matrix A and the right hand side vector $\vec{b}$, both of which are known at each step of the calculation.

Method (32) is simply the standard trapezoidal rule of integration (now referred to as the box method). Formulas (33) and (34) are higher order generalizations of the trapezoidal rule. Method (33) is now often referred to as the "super box" method. We prefer to call these Hermite box methods in general and "nth order Hermite box" method for formulas using the nth derivative of $\vec{F}$.

In this work formula (34) is used. It has the incredibly small truncation error $(\Delta z_i^7/100800)\,\vec{F}^{(7)}(\xi)$ where ξ is some mean value constant. All these formulas can be proved to be absolutely stable so that large step sizes Δz_i can be fully utilized and still achieve accurate results. In fact, solution of equations (28a,b,c) for the planar stagnation point produced 8-significant figure accuracy with 50 points across the interval z belonging to [0,10]. This compares favorably to Rosenhead's (1963) solution to 6 figure accuracy which required about 50 points in the interval [0,5] (about half our step size). Rosenhead's solution used a fourth order method with extrapolation to sixth order.

All the calculations performed in this work used double precision arithmatic and formula (34) with a uniform step size of $\Delta z = 0.1$. Thus, if the maximum value of $|\vec{F}^{(7)}(\xi)|$ is O(1) then the numerical integration errors are

about 10^{-12}. Extensive testing on various step sizes and at single and double precision confirms this estimate.

3.3 CALCULATION OF THE COMPONENTS f AND q

For each value of n equations (28d,e) - (30d,e) all have the form

$$\frac{\partial f_n}{\partial z} + q_n = 0$$

$$\frac{\partial q_n}{\partial z} - g_o q_n = s_{n-1} \qquad (35a,b)$$

where S_{n-1} is a function that depends on lower order terms f_j, q_j, g_j, $j<n$. It is easy to show by the method of variation of parameters that

$$f_n = C_n f_o(z) - \int_o^z l_n(\eta)\, d\eta \qquad (36)$$

$$q_n = -C_n \exp(a(z))/E + l_n(z) \qquad (37)$$

where

$$a(z) = \int_o^z g_o(\eta)\, d\eta \qquad (38)$$

$$f_o(z) = \frac{1}{E} \int_o^z \exp(a(\eta))\, d\eta \tag{39}$$

$$E = \int_o^\infty \exp\,(a(\eta))\, d\eta \tag{40}$$

$$l_n(z) = \int_o^z \exp\,[a(\eta) - a(z)]\, s_n(\eta)\, d\eta \tag{41}$$

and

$$C_n = \int_o^\infty l_n(\eta)\, d\eta\ . \tag{42}$$

All the integrals in equations (36 - 42) were evaluated using the third derivative formula (34). In this case the terms $\vec{F}^{(j)}$ simply denotes derivatives of the desired integrals. For example if one wants to calculate

$$I = \int_o^{z_i} f dz$$

then formula (34) would be

$$I_i = I_{i-1} + \frac{\Delta z_i}{2}(f_i + f_{i-1}) + \frac{\Delta z_i^2}{10}(-f_i' + f_{i-1}') + \frac{\Delta z_i^3}{120}(f_i'' + f_{i-1}'') \ .$$

3.4 RESULTS FOR THE SADDLE POINT

The series expansion method outlined in the previous sections was programmed. A calculation was made for 50 terms of this series. The aim was to apply the techniques expounded by Van Dyke (1984) to determine the nature of the true solution of the problem. The calculations were performed once in single precision and once in double precision to determine the effects of roundoff error. By comparing the results of these two calculations it was found that roundoff errors are probably confined to the last four of the 16 decimal digits of the double precision results. Thus, the accurate numerical integration method (one part in 10^{12}) and stable roundoff behavior indicates that the computed series coefficients may be accurate to 10 or 12 decimal places.

It is not effective to analyze the complete velocity field (h,r,f,q). Instead the wall skin friction component in the attachment line direction (x-direction) is

considered for detailed study. The wall skin friction coefficient C_{fx} is given by

$$C_{fx} = \tau_{wx}/\rho U_o^2$$

$$= \sqrt{\nu}\, e\, \sin_x\, (\partial f/\partial z)_o/U_o^2 \qquad (43)$$

so that

$$U_o^2\, C_{fx}/\sqrt{\nu}\, e\, \sin_x = -q(0) \qquad (44)$$

Thus, the series expansion for q(0) is examined in detail. These results can then also be directly compared to Davey's (1961) results.

The series for q(0) which will be denoted simply by t for simplicity can be written as

$$t = q(0) = \sum_{n=o}^{N} e_n t_n \qquad (45)$$

where N=50, but other, lower, values of N will also be considered. The complete table of coefficients t_n for N=50 is

given in Appendix A. These coefficients are rounded to 10 figures.

The coefficients t_n increase in magnitude and have a sign pattern that indicates complex conjugate singularities near the origin of the complex e-plane. Any complex singularity must be paired with its complex conjugate because the coefficients t_n are all real.

A Domb-Sykes plot (see Van Dyke, 1984) of the coefficients is very irregular and does not give useful information. A similar Domb-Sykes type plot using the root test

$$e_* = \text{limit } |t_n|^{-1/n} \qquad (46)$$

gives an estimate of the radius of convergence e_* of this series. In a Domb-Sykes plot the quantity $|t_n|^{-1/n}$ is plotted versus values of 1/n and extrapolated linearly to (1/n) = 0 (i.e., n=∞). The value so obtained is an estimate of e_*. It was found in this way that

$$e_* \approx 0.55 \ .$$

Thus, the radius of convergence of the series expansion is about 0.55. This does cover a range of values of e for which backflow along the attachment line does occur. Recall that Davey (1961) showed that backflow at the saddle point (i.e., flow away from the saddle point along the attachment line, whereas the outer inviscid flow is towards the saddle point) occurs for e=0.4294. However, the limit e_*=0.55 is a disappointly small fraction of the range e=[0,1] for which the saddle point flow exists.

In order to overcome this limitation on the convergence of the series (45), it can be recast in terms of Pade' fractions (Van Dyke, 1984). This recasting of a series effectively serves as a device to analytically continue t outside the region of convergence. The Pade' fractions capture the singularities that limit convergence as poles in the denominator. Branch point singularities are approximated by a distribution of very weak poles along the branch cuts. These properties of the Pade' fractions emerge automatically from the mere calculation of the coefficients.

Thus, the series (45) is written as

$$t = \sum_{n=o}^{N} e^n t_n = \frac{\sum_{i=o}^{L} a_i e^i}{1 + \sum_{j=1}^{M} b_j e^j} \qquad (47)$$

where L+M=N. By reexpanding the Pade' fraction on the right of equation (47) into a power series about e=0 one can match the coefficients of the powers of e and obtain a linear system of equations for the coefficient a_i and b_j. Once these coefficients are in hand the numerator and denominator are solved for their respective zeroes to determine the zeroes and poles of the Pade' fraction. This type of Pade' analysis can be carried out for all combinations of $0<L+M\leq N$. In most cases only the fractions with $L\simeq M$ are useful.

In the present study the following Pade' fractions were analyzed; (L,M) = (K-1,K), (K,K) and (K,K-1) where $11<K\leq(2N+1)/2$. It was found that the (K-1,K) and (K,K-1) fractions behaved erratically and seemed to converge to useful results only for values of e<0.7. The equal order fraction (K,K) produced consistant and convergent results for values of e fairly close to the limiting value e=1. The (K,K) Pade' fraction for K=25, corresponding to N=50, is tabulated in Appendix A.

The results of this calculation and the analysis of the Pade' fraction indicates the following facts:

(i) The function t(e) has a zero (corresponding to the onset of reverse flow) of e=0.429368226. This number

seems to be correct based on various orders of truncation, numerical integration step size and placement of the outer integration limit z_∞. This value also compares favorably to Davey's value of 0.4294 and the improved value of Cooke and Robins (1970) of e=0.42937.

(ii) The singularities blocking the convergence of the series (45) are a pair of branch points located at

$$e = 0.427 \pm i0.346$$

where $i = \sqrt{-1}$. Note that this gives a radius of convergence $e_* = 0.55$ confirming the value obtained by the root test. There are poles all along two arcs, one from each of the two branch points, extending towards positive values of Real(e). The residue of each of these poles is very small. As the value of K is increased more and more of these poles appear, thus leading to the conclusion that the above singularities are branch points. Unfortunately the irregular behavior of the Domb-Sykes plot prevents the determination of the exponent of these branch points.

(iii) Since the branch points appear for Real(e) > 0, the Euler transformation that maps these points to

infinity is not useful. Thus no information can be obtained by an Euler transformation. However, if the series values of $e<0$ were desired (i.e., the nodal point analysis) then the Euler transformation would yield a useful new series.

(iv) The Pade' fraction has no singularities on $-1 \leq$ Real $(e) \leq 1$ hence it can be used to evaluate t for real values of e. However, the accuracy of these values can only be tested experimentally by monitoring the values of t at varying orders of truncation K. Table II gives the calculated values of t as a function of e for K=10(N=20), K=15(N=30), K=25(N=50) and Davey's values. It can be seen from Table II that convergence of the values of t is very rapid in K for values of $e \leq 0.6$. However, for values of $e>0.6$ the convergence rate with respect to K is fairly slow especially for $e \geq 0.8$. For e=0.9, K=25 (N=50 terms) produces only two significant figures of accuracy. It is important to note that for K=10(N=20) the series expansion method will give reliable values of t only up to e=0.7. For the general case of the attachment line problem the series expansion method is a double series in x and e so that calculating a large number of terms, such as N=50 may not be feasible. Nevertheless, the method can give accurate results with K=10 at least for $e \leq 0.7$

which is substantially within the backflow region e>0.4294.

It should be mentioned that we have also solved this problem by direct numerical integration of the saddle point equations. This calculation confirms Davey's results for all his values of e to the four significant figures that he gives.

In summary, it should be noted that the series expansion method does provide a useful way of evaluating the saddle point flow for values of e at least up to 0.7 with a modest number of terms. The series convergence is blocked by branch points at a radius of about 0.55 and these cannot be removed easily.

In Figure 3 the velocity profile f(z) at the saddle point for e=0.7 is plotted. The profile shows the reversed flow region at the wall and shows that separation occurs on the attachment line ahead of the saddle point. The question that one faces now is whether the saddle point solutions for e>0.4294 have any relevance when separation occurs upstream. This question is to be answered by analyizing the entire attachment line boundary layer.

In the next section the full attachment line boundary layer will be considered. This flow will be calculated in two ways. One way is by direct numerical integation and the other way is by the series and Pade' fraction method. It will be seen that the series method extends the calculations to larger values of e than can be obtained by direct numerical integration.

Section 4

THE FLOW ALONG THE ATTACHMENT LINE-DIRECT NUMERICAL SOLUTION

4.1 DESCRIPTION OF THE FLOW AND NUMERICAL METHOD

The aim now is to solve the complete attachment line problem formulated by equations (12 - 18). The primary question which we wish to answer is the following: Can the boundary layer proceed through the separation point, which occurs upstream of the saddle point, and terminates at the saddle point with Davey's separated solution? Implicit in this question is if this separated boundary layer profoundly affects the external inviscid flow (i.e., $\delta_* \to \infty$ at separation) and viscous/inviscid interactions are required. If the outer potential flow does require modifications in order for the boundary layer to proceed past separation, then Davey's solutions for $e>0.4294$ are irrelevant. Davey (1961) and Cooke and Robins (1970) assumed this to be so. In particular, Cooke and Robins (1970) examined this problem, but for an artificial inviscid flow, for $e<0.4294$ and simply reiterated Davey's assumption that for $e>0.4294$ the boundary layer cannot proceed past the separation point on the attachment line.

It is not at all obvious that Davey's assertion is correct. Separation can occur with the displacement thickness δ_* remaining bounded. Under such a circumstance the separated flow does not, to order $R^{-1/2}$ where R is Reynolds number, disturb the inviscid flow (Klemp and Acrivos, 1976). It is a common occurance in three dimensional symmetry plane boundary layers that the displacement thickness not only remains bounded but in fact decreases as separation is approached. An example of this is given in Part II of this report concerning the leading edge boundary layer on a disk in edgewise flow. The feature that causes the boundary layer thickness to remain bounded even at separation is the very strong lateral outflow to either side of the symmetry plane. These flow features are present in the attachment line boundary layer considered here.

The equations (12 - 18) are solved numerically by starting at the nodal point x=0 and marching the solution in increasing values of x until the saddle point $x=\pi$ is reached. The numerical method used is the standard box method and needs no further elaboration. Reference can be made to Cebeci and Bradshaw (1977) for the details of applying the box method to general boundary layer equations.

It should be noted that for values of e>0.4294 separation of the f component of velocity will occur ahead of

the saddle point $x=\pi$ and thus the numerical method must march against the stream, $f<0$, in part of the boundary layer. This problem can be circumvented by noting that the cases for which $f<0$ have $f << 1$ so that the terms

$$f \frac{\partial f}{\partial x}$$

in equations (14) and (15) can be set to zero when $f \leq 0$. This avoids the unstable phenomena of effectively negative diffusion (i.e., marching upstream instead of downstream). Such a procedure is now called the FLARE approximation. Its accuracy and general validity is not completely quantified so that results obtained using this approximation must be accepted with caution. Also the FLARE approximation may not work for flow velocities $f<0$ whose magnitude exceeds a certain level. For these reasons it is necessary to calculate the flow with $e>0.4294$ with other methods that do not make use of such a crude approximation and that are more robust for larger values of e. This motivated our work to solve equations (12 - 18) by high order perturbation series in e.

4.2 SOME RESULTS OF THE NUMERICAL INTEGRATION

The direct numerical integration method was applied to two cases of nodal to saddle attachment line flow. The

first case was to the flow described by the inviscid flow of equation (1). This calculation resulted in successful integrations from the nodal to the saddle point only for values of $e \leq 0.55$. This range of values of e does encompass the separated flow, but it was felt that the complete boundary layer can be calculated for larger values of e. The value of 0.55 at which the FLARE approximation ceases to work has nothing to do with the value of $e_* = 0.55$ for the convergence of the saddle point series.

The second case considered was the inviscid flow used by Cooke and Robins (1970). Their inviscid flow also corresponded to an attachment line flow between nodal and saddle points, but it did not correspond to any particular geometric shape and thus was somewhat artificial. However it was useful to compare our calculations with theirs, so their case was calculated. Since the results and conclusions are qualitatively the same for either external inviscid flow, the case of Cooke and Robins will suffice to illustrate points.

The Cooke and Robins case was prepared as a short paper and submitted to the Journal of Applied Mechanics. This paper is reproduced in Appendix B. Thus, one can turn to this appendix for the details of the results.

It is sufficient to state here that the boundary layer on the attachment line can indeed be computed through separation all the way to the saddle point for values of e larger than 0.4294. (Note: Since the external inviscid flow has different forms in the present and Cooke and Robins cases, the values of e do not correspond one-to-one on the attachment line. However, at the saddle point the values of e do correspond. Thus e>0.4294 always implies separation ahead of the saddle point, but at different locations for different external inviscid flows.)

As mentioned in Appendix B, it seems reasonable to expect that the boundary layer flow terminating with Davey's saddle point solution exists for even larger values of e. For this reason the e-expansion techniques was used in the next section.

Section 5

PERTURBATION SERIES SOLUTION OF THE ATTACHMENT LINE FLOW

5.1 BASIC FORMULATION AND EXPANSION

In order to both verify and extend the solutions obtained by the direct numerical integration of Section 4, the attachment line equations are now solved by a series expansion in both x and e. The starting point is equations (12 - 18).

First it is convenient to make the change in independent variable from x to s by the transformation

$$s = - \cos x \ . \tag{48}$$

Equations (12 - 16) then become

$$\frac{\partial h}{\partial r} + r = 0 \tag{49a}$$

$$e\left[(1-s^2)\ \frac{\partial f}{\partial s} - sf\right] + \frac{\partial g}{\partial z} + h = 0 \tag{49b}$$

$$e(1-s^2)\ f\ \frac{\partial h}{\partial s} + \frac{\partial r}{\partial z} - gr + h^2 = 1 \qquad (49c)$$

$$\frac{\partial f}{\partial z} + q = 0 \qquad (49d)$$

$$e\left[(1-s^2)\ f\ \frac{\partial f}{\partial s} - sf^2\right] + \frac{\partial q}{\partial z} - gq = -\ es \qquad (49e)$$

The boundary conditions remain equations (17 - 18). Next the vector $\vec{F} = (h,g,r,f,q)^+$ is expanded as

$$\vec{F} = \sum_{n=0}^{N} \sum_{m=0}^{n} e^n s^m \vec{F}_{nm} \ . \qquad (50)$$

By substituting expansion (50) into equations (49) and collecting the appropriate terms of equal powers in $e^n s^m$ one obtains the following perturbation equations:

$$\frac{\partial h_{nm}}{\partial z} + r_{nm} = 0 \qquad (51a)$$

$$\frac{\partial g_{nm}}{\partial z} + h_{nm} = p_{b\,nm} \qquad (51b)$$

$$\frac{\partial r_{nm}}{\partial z} - (g_o r_{nm} + r_o g_{nm} - 2h_o h_{nm})' = p_{cnm} \qquad (51c)$$

$$\frac{\partial f_{nm}}{\partial z} + q_{nm} = 0 \qquad (51d)$$

$$\frac{\partial q_{nm}}{\partial z} - g_o q_{nm} = p_{enm} \qquad (51e)$$

where the prime on the parenthesis in equation (51c) indicates that the term is multiplied by 1/2 for n=m=0. The functions p_{bnm}, p_{cnm} and p_{enm} are defined as follows:

$$p_{bnm} = m\, f_{n-1,m-1} - (m+1)\, f_{n-1,m+1} \qquad (52a)$$

$$p_{cnm} = \delta_{no}\delta_{mo} + \sum_{\ell=o}^{n-1} \sum_{k=o}^{\ell} \Big\{(1-\delta_{\ell o})(g_k r_{n-\ell,m-k} - h_{\ell k} h_{n-\ell,m-k}) - f_{\ell k}\Big[c(m-k+1)\, h_{n-\ell-1,m-k+1} - (m-k-1)\, h_{n-\ell-1,m-k-1}\Big]\Big\} \qquad (52b)$$

and

$$p_{enm} = -\delta_{n1}\delta_{m1} + \sum_{\ell=o}^{n} \sum_{k=o}^{\ell} \Big\{ (1-\delta_{\ell o})\ g_{\ell k}\ q_{n-\ell,m-k}$$

$$- (1-\delta_{\ell n})\ f_{\ell k} \Big[c(m-k+1)\ f_{n-\ell-1,m-k+1}$$

$$- (m-k)\ f_{n-\ell-1,m-k-1} \Big] \Big\} \qquad (52c)$$

where

$$c = \begin{cases} 1 & \text{for } m < n-1 \\ 0 & \text{for } m \geq n-1 \end{cases}$$

The details of the derivation of these equations are straightforward, but somewhat tedious. The main points to note are the following:

(i) Equations 51 and 52 hold for all values of $n \geq 0$ and for $0 \leq m \leq n$ for each n. Furthermore $g_{oo} = g_o$ etc. If the upper limit in one of the sums in Eqs. (52) is less than the lower limit then the sum is null. δ_{ij} is the kronecker delta function.

(ii) For n+m = odd $\vec{F}_{nm}=0$. This greatly reduces the amount of storage required for large values of N. The amount of computer storage available is the main limiting factor on the number N of terms that can be computed.

(iii) The differential operators on the left side of the equations (51) are identical to the differential operators of the saddle point expansion of Section 3. Only the right hand sides of equations (51) are different. Thus the exact same numerical techniques and also about 75% of the computer program for the saddle point expansion can now be carried over to the attachment line equation.

(iv) The boundary conditions on $\vec{F}_{oo} = \vec{F}_{o}$ are the same as Eqs. (28) and those for F_{nm}, n>0 are the same as Eqs. (30).

The numerical procedure for calculating the coefficients $\vec{F}_{nm}$ need no further discussion other than to note that there are many more terms. In fact the number T of terms $\vec{F}_{nm}$ is given by the formula

$$T = \begin{cases} \left[\frac{(N+1)^2}{4}\right] + \left[\frac{N+1}{2}\right] + 1 & \text{for N even} \\ \left[\frac{(N+1)^2}{4}\right] + \left[\frac{N+1}{2}\right] & \text{for N odd} \end{cases}$$

Thus, for N=20, T=121 terms are required. Since F_{nm} is a 5-dimensional vector, and if 100 points in z are retained across the interval $[0,z_\infty]$ then a total of 60500 double precision numbers must be stored. But in order to keep the program complexity and computing times reasonable certain of the components of $\vec{F}'_{nm}$ and $\vec{F}''_{nm}$ must also be stored. This basically doubles the above number of double precision numbers to 120000. Since one double precision number requires 8 bytes of storage a total of about 1 million bytes of storage is required. This amount of storage is about the limit available on our machine. Thus, the present calculation is limited to N=20. However, it is a simple matter to transport our program to a larger machine and obtain results for larger values of N if such a machine becomes available. The computer time required for N=20 is only 15 minutes on a DEC-10.

5.2 RESULTS OF THE PERTURBATION EXPANSION OF THE ATTACHMENT LINE FLOW

A total of N=20 terms (actually 21 terms including n=0) were computed. Again we will illustrate our results by

simply considering the value of $(\partial f/\partial z)_{z=0} = -q(o)$ which is proportional to the skin friction in the attachment line direction. Thus the series

$$q(0) = \sum_{n=o}^{N} \sum_{m=o}^{\eta} e^n s^m \tag{53}$$

is described. It should be noted that the attachment line direction skin friction coefficient $C_{fx} = e\sqrt{\nu}\ \sin xq(0)/U_o^2$.

The series (53) was first summed for each value of s as

$$q_n(0) = \sum_{m=o}^{n} s^m\, q_{nm}(0) \tag{54}$$

to give the series

$$q(0) = \sum_{n=o}^{N} e^n\, q_n(0)\ . \tag{55}$$

This later series is then recast as a Pade' fraction and evaluated for various values of e.

It was found that for $e<0.55$ the series was convergent for all values of s and gave essentially identical results to the direct numerical method of Section 4, even in the separated region. For $e<0.55$, the Pade' analysis was unnecessary since the series converges for all values of s. These, relatively uninteresting results will thus not be shown.

For values of $e>0.55$ it was already indicated that the direct numerical integration method could not proceed beyond the point of separation. However, the series expansion method with N=20 and with the help of the (K,K) Pade' fraction with K=10 did seem to produce accurate values of $q(0)$ for all values of s in $[-1,1]$ i.e., x in $[0,\pi]$ and for $e=0.6$ and possibly also $e=0.65$. Figure 4 shows the plot of $q(0)$ versus x for $e=0.6$, 0.65 and 0.7 obtained by the series method and the numerical integration. In all three cases the direct numerical integration yields values of $q(0)$ which nearly coincide with the values of $q(0)$ obtained by the series up to the point of separation. Even for $e=0.7$, separation is predicted at $x=0.71$ by the direct numerical method and $x=0.714$ by the series method. However, beyond separation the predicted values of $q(0)$ for $e=0.7$ behave in an irregular manner and thus leave some doubt as to the convergence of the series method. It was already seen in the saddle point expansion that N=20 is inadequate to get more

than possibly two significant figures for q(0). There seems to be some indication in Figure 3 that the convergence of the Pade' approximation is poorer just beyond separation than at the saddle point. If this is so, then there is a possibility that the flow does become singular at separation for values of e<1.0 and cannot be continued, without a modification to the external inviscid flow, all the way to the saddle point. In this case Davey's saddle point solutions are irrelevant. However, it does seem clear that the flow on the attachment line does pass smoothly through separation and terminates at the saddle point with Davey's profile for values of e at least up to 0.65. Thus there is a substantial range of flows exhibiting the separated horseshoe vortex that can be calculated by pure boundary layer theory with no viscous/inviscid interactions.

Figure 5 shows a sequence of attachment line direction velocity profiles in the neighborhood of the saddle point for e=0.55. These profiles were calculated using the direct numerical integration. The figure clearly shows the small separated region. Since the attachment line is in the spanwise direction of the cylinder and the main flow direction is around the circumference, the attachment line flow is actually the start of the cross-flow of the main three-dimensional boundary layer of the cylinder. Also since the vorticity generated by the attachment line component of the

velocity is perpendicular to the attachment line, Figure 5 indicates the existence of a streamwise (circumferential) concentrated vortex that will surround the cylinder at the narrow positions.

Section 6

CONCLUDING REMARKS

The calculation described in the previous sections have shown the interesting fact that along the line of attachment on the plane of symmetry of three dimensional flows it is possible to have a separated boundary layer that is determined by the outer inviscid stream corresponding to the body alone. This is an important finding because it indicates that in some cases the horseshoe vortex formed by the boundary layer rollup ahead of an obstruction can still be calculated by boundary layer theory alone. A Navier-Stokes, or even a PNS, calculation is not required to predict this horseshoe vortex.

It was also learned that the FLARE method for computing in the separated region is inadequate if the separation is too large, even though the boundary layer theory still holds. The perturbation method is not a suitable computational tool to deal with practical geometries such as a destroyer bow. Such shapes do not lend themselves to simple one dimensional parameterizations. However a practical method for handling separated flow or the general geometries might be the method of Klemp and Acrivas (1976). This certainly should be investigated. It is important to

develop such calculation methods so that general destroyer bow domes can be treated. This is a necessary step if a rational boundary layer procedure is required for destroyer hulls.

These same comments hold for the case of the root boundary layer of the blade/hub intersection. In this problem it can be seen that a certain amount of filleting can reduce the intersection horseshoe vortex to such a size that it does not disturb in a gross way the body generated potential flow. This is all that is really needed for good fillet design.

On full scale ships the region of laminar flow is likely to be a tiny part of the hull surrounding the nodal point of attachment. Surely the boundary layer will transition far ahead of the saddle point. There is no reason to believe that the attachment line boundary layer could not as easily be calculated for turbulent flow with a suitable turbulence model. However, since the velocity decreases as the saddle point of attachment is approached and since the divergence of the flow is very strong there it may happen that the flow will retransition back to laminar flow before the saddle point is reached. This is an interesting question that needs further investigation and would have serious

implications for the turbulence model in the vicinity of a saddle point of attachment.

Section 7

REFERENCES

Cebeci, T. and Bradshaw, P. (1977), Momentum Transfer in Boundary Layers, McGraw-Hill, New York.

Cooke, J.C. and Robins, A.J. (1970), "Boundary layer flow between nodal and saddle points of attachment," J. Fluid Mech., 41, 823-835.

Davey, A. (1961), "Boundary-layer flow at a saddle point of attachment," J. Fluid Mech., 10, 593.

Groves, N.C. (1981), "An integral prediction method for three-dimensional turbulent boundary layers on rotating blades," Propellers '81, Soc. Nav. Arch. Marine Eng., New York.

Klemp, J.B. and Acrivas, A. (1976).

Rosenhead, L. (ed.) (1963), Laminar Boundary Layers," Oxford.

Van Dyke, M. (1984), "Computer extended series," Ann. Rev. Fluid Mech., 16, 287-309.

Section 8

FIGURES

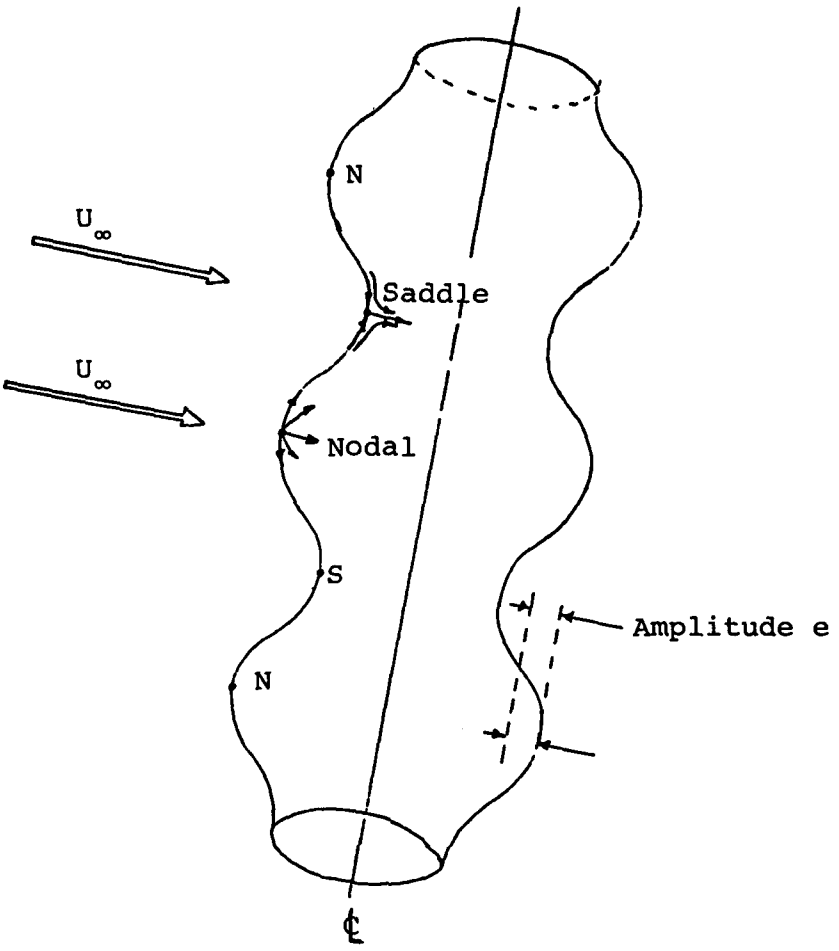

Figure 1. Flow past a corrugated circular cylinder. The nodal points of attachment are denoted by N and the saddle points by S.

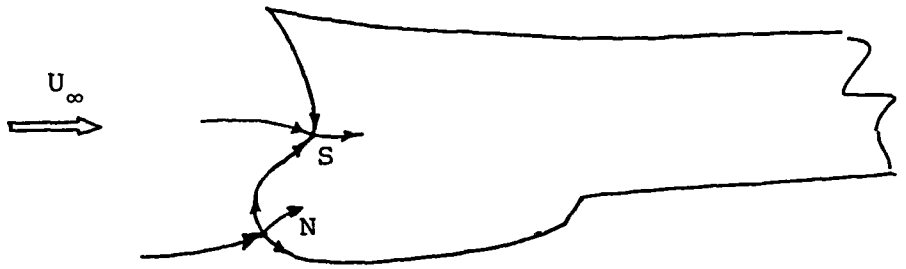

Figure 2. The flow attachment at the bow of a destroyer hull. Point N is a nodal point and S is a saddle point of attachment.

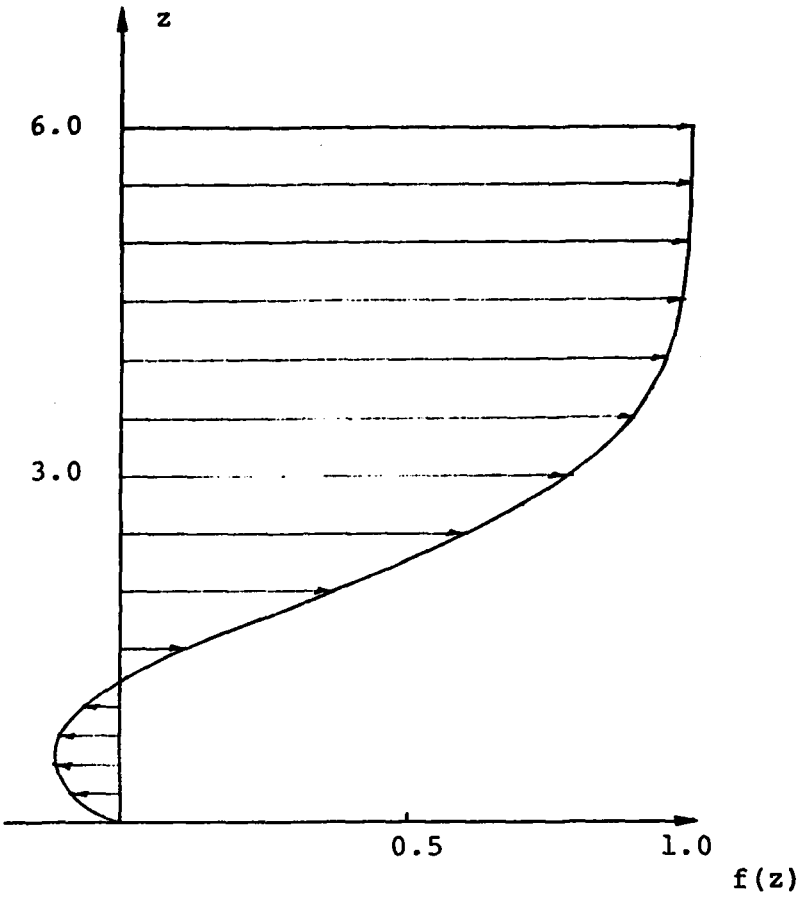

Figure 3. The velocity profile f(z) = u(z)/esinx at the saddle point x=π for e=0.7.

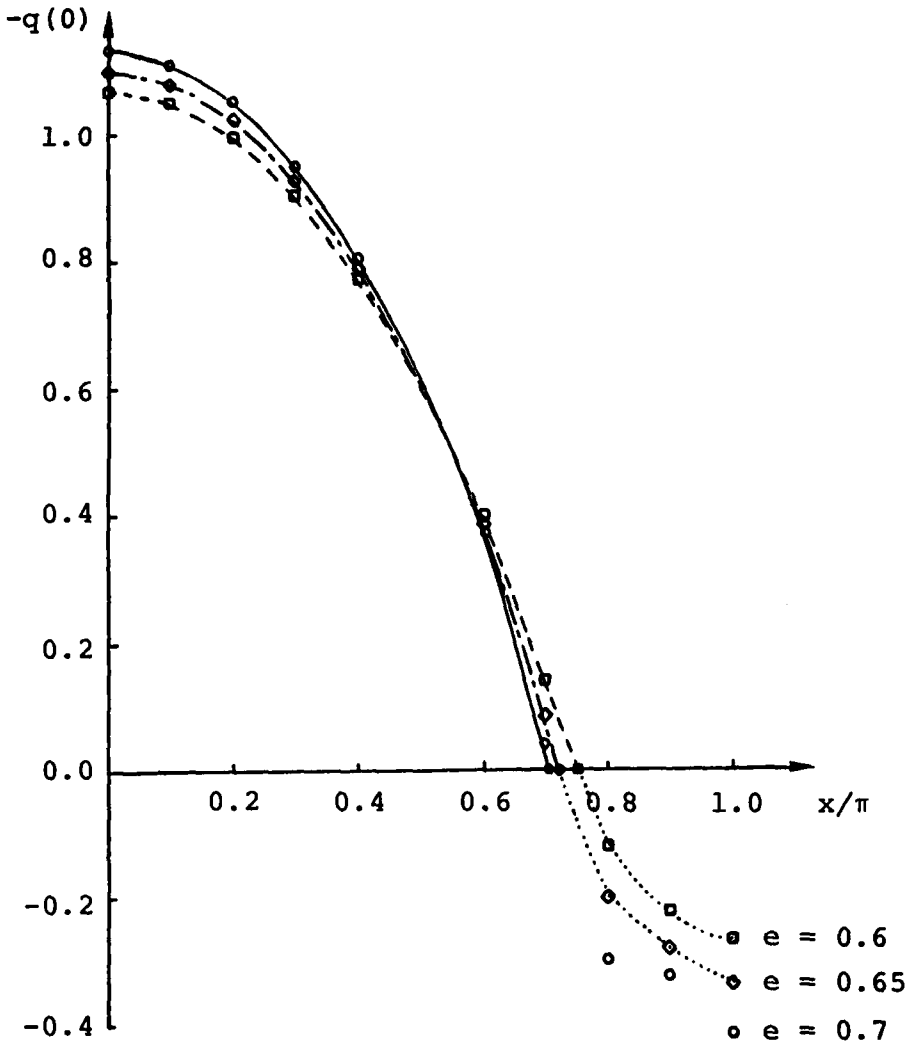

Figure 4. The value of the x-component of the wall skin friction coefficient -q(0) as a function of distance x from the nodal point at x=0 to the saddle point x=π.

e	20 term series	direct numerical
0.6	□	-------
0.65	◇	— - —
0.7	○	———

For e=0.6 and 0.65 the series results have been interpolated by the ... curves to show regular behavior.

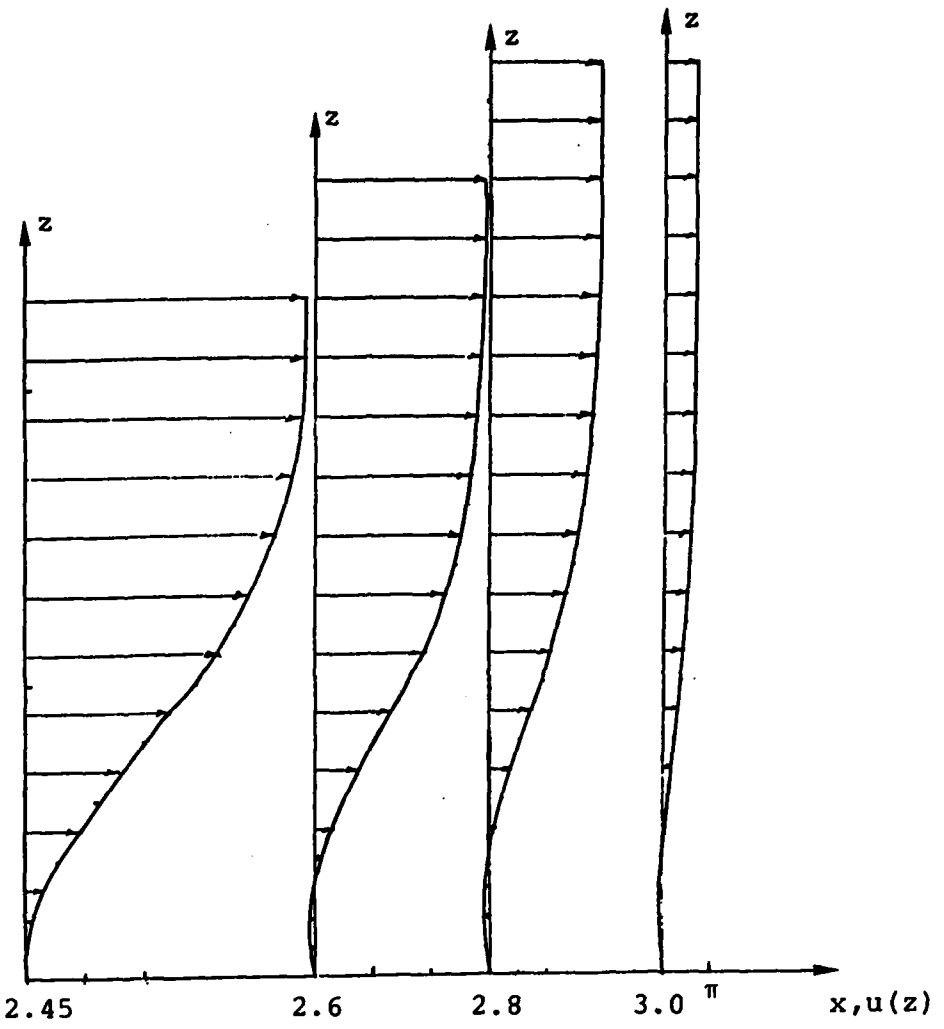

Figure 5. The velocity profiles u(z) for the flow along the attachment line for e=0.55. The saddle point is at x=π.

Appendix A

TABLES OF NUMERICAL RESULTS

SERIES(50)(X)	PADE(25,25)(X) =
-.5704652525D+00*X** 0	-.5704652525D+00*X** 0
.1053234471D+01*X** 1	.7059840489D+01*X** 1
.5398605816D+00*X** 2	-.3739315631D+02*X** 2
.3632211708D+00*X** 3	.1017958962D+03*X** 3
.1048701481D+00*X** 4	-.1083245618D+03*X** 4
-.3171103056D+00*X** 5	-.1660314591D+03*X** 5
-.8735167146D+00*X** 6	.6932322542D+03*X** 6
-.1353168116D+01*X** 7	-.7877205048D+03*X** 7
-.1288116911D+01*X** 8	.1804664342D+03*X** 8
.4580482502D-02*X** 9	-.7824261432D+03*X** 9
.3094025117D+01*X**10	.4189294352D+04*X**10
.7660909416D+01*X**11	-.6161979200D+04*X**11
.1132759345D+02*X**12	.1459220753D+04*X**12
.8686269312D+01*X**13	.2717835772D+04*X**13
-.8003479724D+01*X**14	.3322742735D+04*X**14
-.4416612966D+02*X**15	.1127274425D+04*X**15
-.9239648057D+02*X**16	-.5539762684D+05*X**16
-.1175639805D+03*X**17	.1481042726D+06*X**17
-.4721269869D+02*X**18	-.2032932536D+06*X**18
.2107858533D+03*X**19	.1715036965D+06*X**19
.6922902362D+03*X**20	-.9106075210D+05*X**20
.1223617160D+04*X**21	.2848786425D+05*X**21
.1232028289D+04*X**22	-.4053012796D+04*X**22
-.3106514888D+03*X**23	-.1209159580D+03*X**23
-.4472888238D+04*X**24	.8174016797D+02*X**24
-.1106525063D+05*X**25	-.3876887074D+01*X**25
-.1836242291D+05*X**26	=----------
-.1083520671D+05*X**27	.1000000000D+01*X** 0
.2010132068D+05*X**28	-.1052931093D+02*X** 1
.8712059342D+05*X**29	.4705489693D+02*X** 2
.1747726846D+06*X**30	-.1008951820D+03*X** 3
.2082729818D+06*X**31	.4161824668D+02*X** 4
.3098506788D+05*X**32	.2998708736D+03*X** 5
-.5547394114D+06*X**33	-.6734451159D+03*X** 6
-.1605875604D+07*X**34	.4168034093D+03*X** 7
-.2666760147D+07*X**35	.2120067392D+02*X** 8
-.2312212941D+07*X**36	.1475005815D+04*X** 9
.1949596261D+07*X**37	-.4550740078D+04*X**10
.1251828419D+08*X**38	.3886743493D+04*X**11
.2820746620D+08*X**39	.1381576460D+04*X**12
.3825127696D+08*X**40	-.1000111811D+04*X**13
.1674802350D+08*X**41	-.5412715045D+04*X**14
-.7382586266D+08*X**42	-.1107880567D+05*X**15
-.2554261145D+09*X**43	.7207196025D+05*X**16
-.4704391168D+09*X**44	-.1408489129D+06*X**17
-.4906990721D+09*X**45	.1545824681D+06*X**18
.1316733770D+09*X**46	-.1054640933D+06*X**19
.1912208305D+10*X**47	.4410557307D+05*X**20
.4857460204D+10*X**48	-.9943530505D+04*X**21
.7351166020D+10*X**49	.6315803747D+03*X**22
.4901180938D+10*X**50	.1426783801D+03*X**23
	-.1856963426D+02*X**24
	.2515278745D+00*X**25

Table I

The saddle point expansion coefficients for N=50 series and the (25,25) Pade' expansion. Here X stands for the expansion parameter e in the text.

e	K=10	K=15	K=25	Davey
.0	.57046525	.57046525	.57946525	0.5705
.1	.45937368	.45937368	.45937368	0.4594
.2	.33532784	.33532784	.33532784	0.3353
.3	.19700104	.19700104	.19700104	0.1970
.4	.04596812	.04596814	.04596814	0.0460
.5	-.11150569	-.11150066	-.11150066	-0.1115
.6	-.26689931	-.26659399	-.26659376	-0.2666
.7	-.41834578	-.41301722	-.41297965	-0.4130
.8	-.58709785	-.55046973	-.54931101	-0.5488
.9	-.82489666	-.69458402	-.68365346	-0.6761
1.0	-.12049790	-.89837162	-.85222725	-0.8112

Table II

The values of -q(0) at the saddle point of attachment for various truncations N of the series expansion and the (K,K) Pade' approximation, K=N/2, compared to Davey's numerical results.

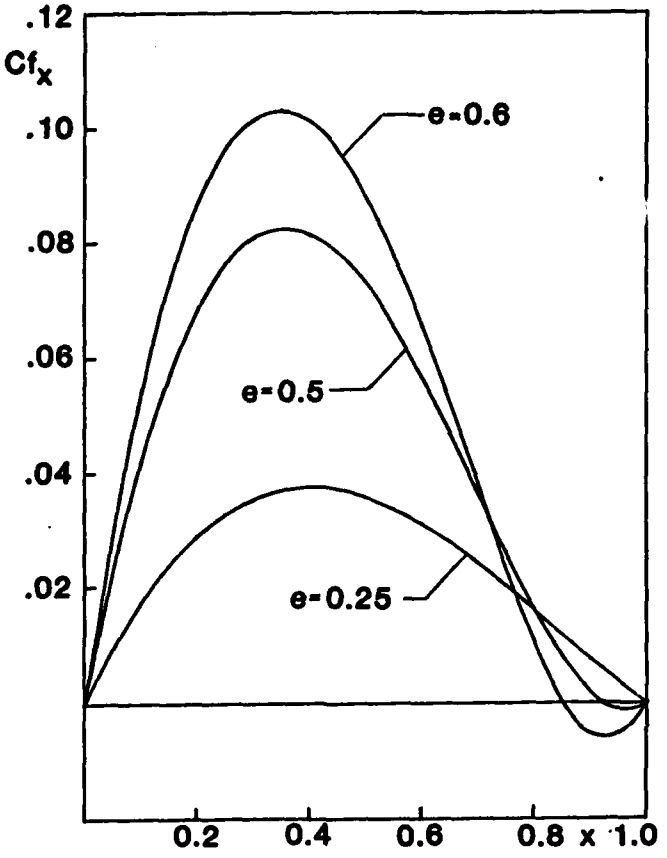
.12
Cf_x
.10
.08
.06
.04
.02
e=0.6
e=0.5
e=0.25
0.2
0.4
0.6
0.8
x 1.0

Part II

THE BOUNDARY LAYER ON AN OBLATE SPHERIOD AT AN ANGLE OF ATTACK

Section 1

INTRODUCTION

The aim of this research project was to investigate leading edge boundary layers on wings and propeller blades. The reason for this investigation is that existing three dimensional boundary layer methods (see Groves, 1981, Groves and Chang, 1985, Cebeci, 1985) do not account properly for such leading edge boundary layers. For example, Groves (1981) simply neglects the leading edge and begins the calculation on the face of the blade with flat plate turbulent boundary layer data. Groves and Chang (1985) assume that the leading edge is wedge shaped and start their calculation with basically the Falkner-Skin similarity profiles. However, for subsonic flows wing and blade leading edges are rounded, not sharp. Cebeci (1985) mentions, in his review of wing boundary layers, only the case where the leading edge is a symmetry plane. In this case the leading edge is an attachment line along which the crossflow pressure gradient vanishes. This reduces the boundary layer equations to quasi-three dimensional form that can be solved separately (as initial conditions) from the remaining three dimensional equations over the rest of the surface. Cebeci (1985) alludes to the assumption that for wings this type of leading edge condition is approximately true even for small angles of

attack. This assumption is probably adequate for fairly high aspect ratio wings with straight leading edges. However, for low aspect ratio wings at moderate angles of attack, for marine propellers and even for the vicinity of the wing tip of high aspect ratio wings the attachament line curves substantially off the leading edge and is not a symmetry plane. Thus, Cebeci's assumption would not be valid in these situations.

The aim was in fact to examine the leading edge flow in the vicinity of a wing or blade tip. This leading edge flow is what initiates the rollup of the tip vortex. It seems appropriate then to study the leading edge boundary layer on a flat oblate spheroid in edgewise flow as depicted in Figure 1. (Figure 1 shows a rather fat oblate spheroid only for the purpose of more clearly depicting some of the details.) This configuration was chosen so that the boundary layer emanating from the front stagnation point would proceed directly to the rounded tip area without having to pass over a large span of basically two-dimensional flow that is relatively benign as concerns the phenomena under consideration here.

A second reason for choosing the oblate spheroid is that its geometry and potential flow is analytically

described. This allows us to concentrate on the boundary layer theory without having to deal with complicated numerical geometry and potential flow codes. Figure 1 shows an example of an oblate spheroid in relation to the oncoming stream whose magnitude is U_∞ and angle of attack is α_*. Also a surface, nonorthogonal, coordinate system used for boundary layer calculations is shown. In the course of this investigation, several different surface coordinate systems had to be used. All these are easily described in terms of the fundamental elliptic coordinate describing the spheroid and its potential flow.

The following plan describes the contents of this report. Section 2 contains the basic spheroid geometry, potential flow, various surface coordinate systems, the formulation of the three-dimensional boundary layer equations in nonorthogonal surface coordinates and the numerical procedures for solving the boundary layer equations. Section 3 describes how boundary layer calculation methods must start. Sections 4 and 5 describe and discuss the results obtained. Section 6 contains some concluding remarks and prognosis for continued effort on the problem.

Section 2

THE GEOMETRY AND BASIC EQUATIONS FOR FLOW OVER AN OBLATE SPINNING SPHEROID

2.1 GEOMETRY AND POTENTIAL FLOW

The geometry of a spheroid, or any other body, is most easily described in terms of parametric coordinates referred back to a global cartesion reference frame. Figure 1 shows an oblate spheroid with the global cartesian (x,y,z) reference frame placed at its centroid. Then the surface of this spheroid, whose half-thickness along the x-axis is τ and whose radius in the y-z plane is 1, can be described in vector form as

$$\vec{R}(\mu,\omega) = \tau\mu\vec{i} + \sqrt{1-\mu^2}\,(\sin\omega\vec{j} + \cos\omega\vec{k}) \qquad (1)$$

where $(\vec{i},\vec{j},\vec{k})$ are the unit vectors corresponding to (x,y,z), (μ,ω) are the orthogonal elliptic coordinates on the surface of the spheroid and $\vec{R}(\mu,\omega)$ is the position vector from the origin of the (x,y,z) frame to a point (μ,ω) on the surface. The length scale of this spheroid is the radius in the y-z plane which has been normalized to 1.

The potential flow whose onset velocity is $\vec{U}_\infty$ in the x-z plane can be found in Durand Vol. 1 (1963). Only the surfaces velocities are needed in this work so that only the reduced formulas are given here. Thus the surface velocity is

$$\vec{V} = U_\mu \vec{e}_\mu + U_\omega \vec{e}_\omega \tag{2}$$

where

$$\left.\begin{aligned} U_\mu &= (\mu\sqrt{1-\gamma^2} - \alpha\sqrt{1-\mu^2})/\sqrt{\tau^2+\lambda^2\mu^2} \\ U_\omega &= \gamma \quad , \quad \gamma = \sin\omega \quad , \quad \lambda^2=1=\tau^2 \end{aligned}\right\} \tag{3}$$

$$\left.\begin{aligned} \vec{e}_\mu &= [\tau\vec{i} - \mu(\sin\omega\vec{j} + \cos\omega\vec{k})/\sqrt{1-\mu^2}]/h_\mu \\ \vec{e}_\omega &= \cos\omega\vec{j} - \sin\omega\vec{k} \end{aligned}\right\} \tag{4}$$

$$\left.\begin{aligned} h_\mu &= \sqrt{\tau^2+\lambda^2\mu}/\sqrt{1-\mu^2} \\ h_\omega &= \sqrt{1-\mu^2}/\cos\omega \end{aligned}\right\} \tag{5}$$

and α is proportional to the angle of attack. In terms of the angle of attack α_* defined as

$$\alpha_* = \frac{\vec{U}_\infty \cdot \vec{i}}{\vec{U}_\infty \cdot \vec{k}} \tag{6}$$

the value of α is

$$\alpha = 2\alpha_*[\lambda(2-\tau^2) - \tau\cot^{-1}(\tfrac{\tau}{2})]/[\lambda\tau-\cot^{-1}(\tfrac{\tau}{2})] \tag{7}$$

The choice of the proper surface coordinate system in which to perform boundary layer calculations is a delicate issue. The choice depends not only on the global but also on the local topology of the surface. For example, in the vicinity of the stagnation point of attachment it is easiest to deal with a local polar coordinate system in most cases. This is particularly true for bodies whose topology near the stagnation point is nearly spherical, i.e., the curvature in every direction is about the same order of magnitude. However, as was discovered in this work, for a flattened body such as a blade or wing, or disk, such a system is not suitable. Instead a locally rectangular system needs to be used.

In this work the basic elliptic system was not used because of the pole at the top and bottom ($x=\pm\tau$) of the disk. Instead two other surface systems were used. One system put the poles at the nose and tail ($z=\pm 1$) at the edge of the disk

and the other system put the poles at the tips ($y=\pm 1$). We shall refer to these coordinate systems as C_1 and C_2 respectively. In order to use the system C_1 when the flow is at an angle of attack, which moves the front stagnation point off the pole, a different transformation, given by Cebeci, Khattab and Stewartson (1981) was used. This combined system will be referred to as C_{1c}.

It is best to leave the description of these coordinate systems to sections where they are applied. At present the general three dimensional laminar boundary layer equations will be given for general nonorthogonal coordinate systems. In fact, the entire development and computer coding in this research effort was carried out for the general case, so that other coordinate systems, body geometries and potential flows could be easily incorporated.

2.2 THE BOUNDARY LAYER EQUATIONS

The general three-dimensional boundary layer equations in nonorthogonal coordinates can be found in several sources, for example, Squire (1955). Let (r,t,n) be such a general nonorthogonal surface coordinate system. The (r,t) coordinates lie in the surface and n can be assumed to be an arclength coordinate tangent to the body normal. Then the

metric equation for an element ds of arclength in this coordinate system is

$$ds^2 = h_r^2\, dr^2 + h_t^2\, dt^2 + 2g\,dr\,dt + dn^2 \ . \qquad (8)$$

The position $\vec{R}$ of any point on the body surface referred to the origin of the global cartesian reference frame is a function of (r,t) and can be written as

$$\vec{R} = \vec{R}(r,t) = x(r,t)\vec{i} + y(r,t)\vec{j} + z(r,t)\vec{k} \ . \qquad (9)$$

The functions x(r,t), y(r,t) and z(r,t) specify this coordinate system and thus are sufficient to calculate any geometric quantity needed. In particular, knowledge of equation (9) allows one to calculate the unit vectors $\vec{e}_r$ and $\vec{e}_t$ in the directions of r and t respectively. Then the surface potential flow velocity $\vec{V}$ can be written as

$$\vec{V} = U_r\vec{e}_r + U_t\vec{e} \ . \qquad (10)$$

One should be careful to note that the components U_r and U_t cannot be obtained from $\vec{V}$ described in an orthogonal frame, such as equation (2), by simple projections. Suppose that $\vec{V}'=\vec{V}$ is described in some other reference frame and the components U_r and U_t are needed. Then the proper components in the (r,t) system are calculated by the formulas

$$U_r = \frac{(\vec{V}' \times \vec{e}_t) \cdot \vec{n}}{|\vec{n}|^2} \vec{e}_r \qquad (11a)$$

$$U_t = - \frac{(\vec{V}' \times \vec{e}_r) \cdot \vec{n}}{|\vec{n}|^2} \vec{e}_t \qquad (11b)$$

where $\vec{n} = \vec{e}_r \times \vec{e}_t$.

Let (u,v,w) denote the boundary layer velocity components in the (r,t,n) directions respectively then the boundary layer equations are the following:

The continuity equation is

$$\frac{1}{h_r} \frac{\partial u}{\partial r} + \frac{1}{h_t} \frac{\partial v}{\partial t} + \frac{\partial w}{\partial n} + uC_r + vC_t = 0 \qquad (12a)$$

The r-momentum equation is

$$\frac{u}{h_r} \frac{\partial u}{\partial r} + \frac{v}{h_t} \frac{\partial u}{\partial t} + w \frac{\partial u}{\partial n} + u^2 e_1 + v^2 e_2$$

$$+ uve_3 - 2\Omega_n \left(\frac{h_t h_r}{p} + \frac{g}{p}\right) = - \frac{h_t^2 h_r}{p^2} \frac{\partial P}{\partial r}$$

$$+ \frac{g h_r}{p^2} \frac{\partial P}{\partial t} + \nu \frac{\partial^2 u}{\partial n^2} \qquad (12b)$$

The t-momentum equation is

$$\frac{u}{h_r}\frac{\partial v}{\partial r} + \frac{v}{h_t}\frac{\partial u}{\partial t} + w\frac{\partial u}{\partial n} + u^2 f_1 + v^2 f_2$$

$$+ uvf_3 + 2\Omega_n\left(\frac{h_t h_r}{p} + \frac{g}{p}\right) = \frac{gh_t}{p^2}\frac{\partial P}{\partial t}$$

$$- \frac{h_r^2 h_t}{p^2}\frac{\partial P}{\partial t} + \nu\frac{\partial^2 v}{\partial n^2} \qquad (12c)$$

with boundary conditions

$$u=v=w=0 \text{ at } n=0$$

and (12d)

$$u = U_r,\ v = U_t \text{ at } n=\infty$$

These equations have been written in terms of a rotating coordinate system with the rotation rate vector $\vec{\Omega}$ whose magnitude is Ω. The component of $\vec{\Omega}$ in the direction normal to the surface is denoted by Ω_n. The pressure P in these equations is the reduced pressure

$$P = \tilde{P} - \frac{1}{2}\Omega^2 R^2 \qquad (13)$$

where R is the perpendicular distance from the point on the surface to the axis of rotation, $\tilde{P}$ is the Bernoulli pressure obtain from

$$\tilde{P}_o - \tilde{P} = \frac{1}{2} \vec{V} \cdot \vec{V}$$

and $\vec{V} = U_r \vec{e}_r + U_t \vec{e}_t$ is referred to the rotating reference frame.

The coefficients of equations (12) are defined in terms of the surface geometry (the metrics h_r, h_t and g) as follows:

$$p^2 = h_r^2 h_t^2 - g^2$$

$$C_r = \left[(h_t^2 - \frac{p^2}{h_r^2})\frac{\partial h_r}{\partial r} + h_r h_t \frac{\partial h_t}{\partial r} - \frac{g}{h_r}\frac{\partial g}{\partial r}\right]/p^2$$

$$C_t = \left[h_r h_t \frac{\partial h_r}{\partial t} + (h_r^2 - p^2/h_t^2) \frac{\partial h_t}{\partial t} - \frac{g}{h_t}\frac{\partial g}{\partial t}\right]/p^2$$

$$e_1 = h_r g\left[\frac{1}{h_r}\frac{\partial h_r}{\partial t} + \frac{g}{h_r^3}\frac{\partial h_r}{\partial r} - \frac{1}{h_r^2}\frac{\partial g}{\partial r}\right]/p^2$$

$$e_2 = h_r\left[\frac{\partial g}{\partial t} - h_t \frac{\partial h_t}{\partial r} - \frac{g}{h_t}\frac{\partial h_t}{\partial t}\right]/p^2$$

$$e_3 = h_r h_t \left[(1 + \frac{g^2}{h_r^2 h_t^2}) \frac{\partial h_r}{\partial t} - \frac{2g}{h_r h_t}\frac{\partial h_t}{\partial r}\right]/p^2$$

$$f_1 = h_t\left[\frac{\partial g}{\partial r} - h_r \frac{\partial h_r}{\partial t} - \frac{g}{h_r}\frac{\partial h_r}{\partial r}\right]/p^2$$

$$f_2 = gh_t\left[\frac{1}{h_t}\frac{\partial h_t}{\partial r} + \frac{g}{h_t^3}\frac{\partial h_t}{\partial t} - \frac{1}{h_t^2}\frac{\partial g}{\partial t}\right]/p^2$$

$$f_3 = h_r h_t\left[\left(1 + \frac{g^2}{h_r^2 h_t^2}\right)\frac{\partial h_t}{\partial r} - \frac{2g}{h_r h_t}\frac{\partial h_r}{\partial t}\right]/p^2$$

Although equations (14) appear formidable and complicated, these coefficients depend only on the geometry of the surface and the coordinate system used to represent this geometry. At the actual calculation stage it is not difficult to write a subroutine that evaluates these terms for whatever geometric representation is available. This part of the calculation can be kept isolated from the details of the boundary layer calculation method.

The boundary layer equations (13b and c) are nonlinear. Thus in any procedure for solving these equations an iterative approach is required. This iterative approach can be implemented at the present analytical stage or later at the numerical stage after the equations (13) have been approximated by finite differences. It seems a little easier to formulate the iterative scheme at this stage.

Nonlinear terms are decomposed by Newton's method in which it is assumed approximate values of the dependent variables are available because of the iteration procedure. Thus typical terms such as u^2, $u\frac{\partial u}{\partial r}$ and uv are replaced by the expressions

$$u^2 = 2\bar{u}u - \bar{u}^2$$

$$u\frac{u}{r} = \bar{u}\frac{\partial u}{\partial r} + \frac{\partial \bar{u}}{\partial r}u - \bar{u}\frac{\partial \bar{u}}{\partial r} \qquad (15)$$

$$uv = \bar{u}v + \bar{v}u - \bar{u}\bar{v} ,$$

where the overbar denotes that the quantity is known from the prior iteraton or as an initially guessed quantity. Note that the above expressions are identities if $\bar{u}$=u etc.

Furthermore it will be easier to work with the equations in first derivative form. Thus, the new variables a and b are defined by the equations

$$\frac{\partial u}{\partial n} + a = 0$$

$$\frac{\partial v}{\partial n} + b = 0 . \qquad (16)$$

By substituting expressions (15) and (16) in the appropriate places in equations (12) and rearranging the

terms, the boundary layer equations can be written in the compact form

$$\nu \frac{\partial \vec{X}}{\partial n} + A \cdot \frac{\partial \vec{X}}{\partial r} + B \cdot \frac{\partial \vec{X}}{\partial t} + C \cdot \vec{X} = \vec{R} \qquad (17)$$

where

$$\vec{X} = (a,b,w,u,v)^{+}$$

$$A = \begin{bmatrix} 0 & 0 & 0 & 0 & 0 \\ 0 & 0 & 0 & 0 & 0 \\ 0 & 0 & 0 & h_r^{-1} & 0 \\ 0 & 0 & 0 & uh_r^{-1} & 0 \\ 0 & 0 & 0 & 0 & uh_r^{-1} \end{bmatrix}$$

$$B = \begin{bmatrix} 0 & 0 & 0 & 0 & 0 \\ 0 & 0 & 0 & 0 & 0 \\ 0 & 0 & 0 & 0 & h_t^{-1} \\ 0 & 0 & 0 & vh & 0 \\ 0 & 0 & 0 & 0 & vh_t^{-1} \end{bmatrix}$$

$$C = \begin{bmatrix} 0 & 0 & 0 & 1 & 0 \\ 0 & 0 & 0 & 0 & 1 \\ 0 & 0 & 0 & C_r & C_t \\ -\bar{w} & 0 & a & C_1 & C_2 \\ 0 & -\bar{w} & b & C_3 & C_4 \end{bmatrix}$$

$$R = (0,0,0,R_4,R_5)^+$$

and where

$$C_1 = \frac{1}{h_r}\frac{\partial \bar{u}}{\partial r} + 2ue_1 + ve_3$$

$$C_2 = \frac{1}{h_t}\frac{\partial \bar{u}}{\partial t} + 2\bar{v}e_2 + \bar{u}e_3 - 2\Omega_n\left(\frac{h_t h_r}{p} + \frac{g}{p}\right)$$

$$C_3 = \frac{1}{h_r}\frac{\partial \bar{v}}{\partial r} + 2\bar{u}f_1 + \bar{v}f_3 + 2\Omega_n\left(\frac{h_t h_r}{p} + \frac{g}{p}\right)$$

$$C_4 = \frac{1}{h_t}\frac{\partial \bar{v}}{\partial t} + 2\bar{v}f_2 + \bar{u}f_3$$

$$R_4 = -\frac{h_t^2 h_r}{p^2}\frac{\partial P}{\partial r} + \frac{h_r}{p^2}\frac{\partial P}{\partial t} + \frac{\bar{u}}{h_r}\frac{\partial \bar{u}}{\partial r} + \frac{\bar{v}}{h_t}\frac{\partial \bar{u}}{\partial t}$$

$$+ \bar{u}^2 e_1 + \bar{v}^2 e_2 + \bar{u}\bar{v}e_3 - \bar{w}\bar{a}$$

$$R_5 = \frac{gh_t}{p^2}\frac{\partial P}{\partial r} - \frac{h_r^2 h_t}{p^2}\frac{\partial P}{\partial t} + \frac{\bar{u}}{h_r}\frac{\partial \bar{v}}{\partial r} + \frac{\bar{v}}{h_t}\frac{\partial \bar{v}}{\partial t}$$

$$+ \bar{u}^2 f_1 + \bar{v}^2 f_2 + \bar{u}\bar{v}f_3 - \bar{w}\bar{b}$$

It is undesirable to deal directly with equations (17). In order to circumvent some of the numercial difficulties associated with boundary layer growth and special situations of stagnation points, symmetry plane or attachment lines, it is desirable to transform some of the dependent and independent variables. Suppose that the t-direction is the main downstream flow direction and that S is the arclength in the t direction. Furthermore suppose that each of the components of $\vec{X}$ is rescaled by some function of r and t only.

Thus, consider the transformations

$$r=r,\ t=t,\ \zeta=n/\sqrt{S\nu} \tag{18}$$

$$\vec{X} = D(r,t,\sqrt{\nu})\cdot\vec{Y} \tag{19}$$

where D is a diagonal matrix.

Then equation (17) becomes

$$\frac{\partial\vec{Y}}{\partial\zeta} + \tilde{A}\cdot\frac{\partial\vec{Y}}{\partial r} + \tilde{B}\cdot\frac{\partial\vec{Y}}{\partial t} + \tilde{C}\cdot\vec{Y} = \vec{T} \tag{20}$$

where

$$\tilde{A} = (A \cdot D + \frac{d\zeta}{dr} D) \sqrt{S}$$

$$B = (B \cdot D + \frac{d\zeta}{dr} D) \sqrt{S} \qquad (21)$$

$$C = (C \cdot D + A \cdot \frac{\partial D}{\partial r} + B \cdot \frac{\partial D}{\partial t}) \sqrt{S}$$

$$\vec{T} = \sqrt{S} \ \vec{R} \ .$$

The equations (20) are handled numerically. By structuring the computer code to deal with equation (20) and delegating to subroutines the calculation of the various coefficient matrices in inverse order in which the terms are presented above, a code is developed that is not too difficult to change for different body geometry, potential flow and coordinate system.

In the next section the general numerical algorithm for solving equation (20) is described. Following that section the specific cases dealt with in this study will be described.

AD-A163 309 ASPECTS OF THE CALCULATION OF BOUNDARY LAYERS ON SHIPS' 2/2
(U) SCIENCE APPLICATIONS INTERNATIONAL CORP ANNAPOLIS
MD C H VON KERCZEK DEC 85 SAIC-85/1158
UNCLASSIFIED N00014-82-C-0599 F/G 20/4 NL

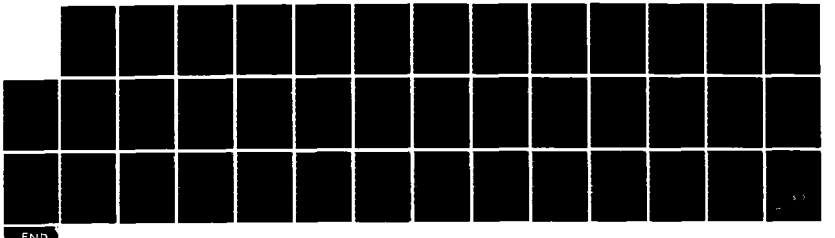

END

FILMED

DTIC

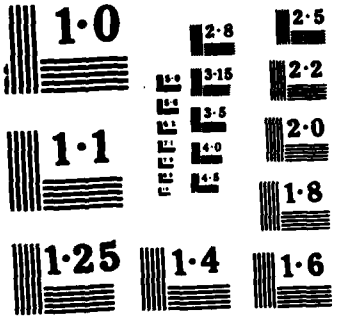

2.3 THE NUMERICAL METHOD

A three dimensional rectangular grid is erected in the (r,t,ζ) coordinate system. One cell of this grid system is shown in Figure 2. In this grid the r-coordinate is partitioned as $\{r_i\}$, the t-coordinate as $\{t_j\}$ and the ζ coordinate as $\{\zeta_k\}$. The value of any function F at a grid point is denoted by $F_{i,j,k}$. It is assumed that the main flow direction is towards increasing values of r and t so that the convective operator $\tilde{A}\cdot\frac{\partial}{\partial r} + \tilde{B}\cdot\frac{\partial}{\partial t}$ in equation (20) is marched foreward in r and t. This means that if values of $\vec{Y}$ are known at stations (i,j,k), (i,j+1,k), (i+1,j,k) for all values of k then the values of $\vec{Y}$ can be calculated at all k of station (i+1,j+1,k). The finite difference equations are then obtained simply by a three-dimensional trapezoidal rule integration over the box with corners (i,j,k), (i,j+1,k), (i+1,j,k), (i+1,j+1,k), (i,j,k+1), (i,j+1,k+1), (i+1,j,k+1) and (i+1,j+1,k+1). This is called the box method.

A simple way to view this method is to consider that the differential equation (20) is evaluated at the center of the box. Thus, the value of quantity at the center of the box is denoted by an asterisks subscript, such as F_*. Thus the value of $\vec{Y}$ at the center of the box is simply obtained by averaging the values over the eight corners of the box. Similarly, the value of a derivative at the center

of the box is obtained by averaging the two-point differences formed at four appropriate edges of the box.

In order to simplify the notation the following scheme will be used. The triple index (i,j,k) is replaced by a double index (l,k) where l = 1,2,3, or 4 corresponding to the four points (i+1,j+1), (i,j+1), (i,j) and (i+1,j). Thus, by looking down onto the (r,t) plane a typical face of the box at level k is shown below.

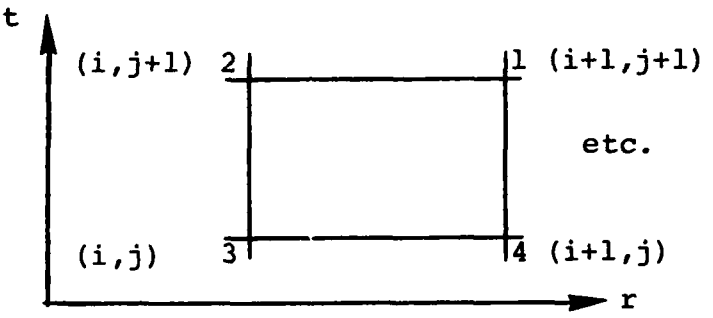

The numbering l increases by proceeding counter-clockwise around the box.

Thus, the various finite difference formulas can be written as follows:

$$\vec{Y}_* = \left[(\vec{Y}_{1,k}+\vec{Y}_{1,k+1}) + (\vec{Y}_{2,k}+\vec{Y}_{2,k+1}+\vec{Y}_{3,k} + \vec{Y}_{3,k+1}+\vec{Y}_{4,k}+\vec{Y}_{4,k+1})\right]/8$$

$$= (\vec{Y}_{1,k}+\vec{Y}_{1,k+1})/8 + \vec{Y}_{*a}/8 \ . \qquad (22a)$$

We split off the values of Y_{*a} at the points 1 = 2,3, and 4 and lump them into the single term Y_{*a} because these are known values. This procedure is followed for the evaluation of all the terms in the equation (20). Hence:

$$\left.\frac{\partial \vec{Y}}{\partial r}\right|_{*} = \frac{1}{4\Delta r_i}\left[(\vec{Y}_{1,k}-\vec{Y}_{2,k}) + (\vec{Y}_{1,k+1}-\vec{Y}_{2,k+1})\right.$$

$$\left. + (\vec{Y}_{4,k}-\vec{Y}_{3,k}) + (\vec{Y}_{4,k+1}-\vec{Y}_{3,k+1})\right]$$

$$= \frac{1}{4\Delta r_i}(\vec{Y}_{1,k}-\vec{Y}_{2,k}) + \frac{1}{4\Delta r_i}\vec{Y}_{*r} \qquad (22b)$$

$$\left.\frac{\partial \vec{Y}}{\partial t}\right|_{*} = \frac{1}{4\Delta t_j}\left[(\vec{Y}_{1,k}-\vec{Y}_{4,k}) + (\vec{Y}_{1,k+1}-\vec{Y}_{4,k+1})\right.$$

$$\left. + (\vec{Y}_{2,k}-\vec{Y}_{3,k}) + (\vec{Y}_{2,k+1}-\vec{Y}_{3,k+1})\right]$$

$$= \frac{1}{4\Delta t_j}(\vec{Y}_{1,k}+\vec{Y}_{1,k+1}) + \frac{1}{4\Delta t_j}\vec{Y}_{*t} \qquad (22c)$$

$$\left.\frac{\partial \vec{Y}}{\partial \zeta}\right|_{*} = \frac{1}{4\Delta \zeta_k}\left[(\vec{Y}_{1,k+1}-\vec{Y}_{1,k}) + (\vec{Y}_{2,k+1}-\vec{Y}_{2,k})\right.$$

$$\left. + (\vec{Y}_{3,k+1}-\vec{Y}_{3,k}) + (\vec{Y}_{4,k+1}-\vec{Y}_{4,k})\right]$$

$$= \frac{1}{4\Delta \zeta_k}(\vec{Y}_{1,k+1}-\vec{Y}_{1,k}) + \frac{1}{4\Delta \zeta_k}\vec{Y}_{*\zeta} \qquad (22d)$$

The matrices $\tilde{A}$, $\tilde{B}$ and $\tilde{C}$ and the vector $\vec{T}$ are evaluated at the center, $*$, of the box simply by evaluating each element of the matrix at the center using the formulas (22). These matrices are then denoted by the asterisk subscript.

The result is that the finite difference equation corresponding to equation (20) is the following:

$$\hat{A} \cdot \vec{Y}_{l,k} + \hat{B} \cdot \vec{Y}_{l,k+1} = \vec{L} \tag{23}$$

where

$$\hat{A} = - I + \Delta\zeta_k \left(\tilde{A}_*/\Delta r_i + \tilde{B}_*/\Delta t_j + \tilde{C}_*/2\right) \tag{24a}$$

$$\hat{B} = I + \Delta\zeta_k \left(\tilde{A}/\Delta r_i + \tilde{B}_*/\Delta t_j + \tilde{C}_*/2\right) \tag{24b}$$

$$\vec{L} = \delta\Delta\zeta_k \vec{T}_* - \vec{Y}_{*\zeta} - \Delta\zeta_k \left(\frac{1}{\Delta r_i}\tilde{A}_* \cdot \vec{Y}_{*r} + \frac{1}{\Delta t_j}\tilde{B}_* \cdot \vec{Y}_{*t} - \frac{1}{2}\tilde{C}_* \cdot \vec{Y}_{*a}\right) \tag{24c}$$

with $\delta = 4$.

Thus, the system of algebraic equations (23) for $k=1,2,\ldots, K_{T-1}$, where K_T is the total number of grid pints in the ζ-direction, together with the boundary conditions can be solved for the K_T unknown vectors $\vec{Y}_{lk}$.

It may be necessary to modify this numerical method when negative crossflow is encountered. Negative crossflow refers to the t-component of velocity, v, becoming negative. In order to maintain the requirements of the zone of influence and dependence the box method is modified to the zig-zag box as follows. In the diagram below the (i,j) finite difference molecule at level k is depicted. The point, *, at which the equations are evaluated is now on the r-grid line between r_i and r_{i+1}. Again, it is assumed that calculation has provided values at all i grid points and at all i+1 grid points up to (i+1,j).

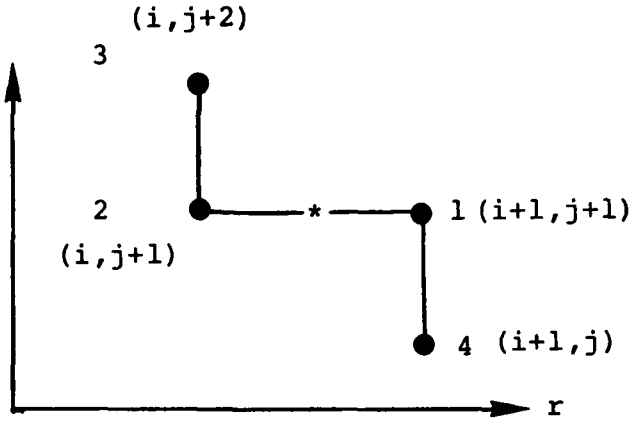

Now it is assumed that 1=3 corresponds to the point (i,j+2). The finite difference formulas need now only be evaluated by averaging over the single face (1,k), (1,k+1), (2,k) and (2,k+1) except for the t derivative. Thus one has

$$\vec{Y}_* = [(\vec{Y}_{1,k} + \vec{Y}_{1,k+1}) + (\vec{Y}_{2,k} + \vec{Y}_{2,k+1})]/4$$

$$= (\vec{Y}_{1,k} + \vec{Y}_{1,k+1})/4 + \vec{Y}_{*a}/4 \qquad (25a)$$

$$\left.\frac{\partial \vec{Y}}{\partial r}\right|_* = \frac{1}{2\Delta r_i}\left[(\vec{Y}_{1,k} - \vec{Y}_{2,k}) + (\vec{Y}_{1,k+1} - \vec{Y}_{2,k+1})\right]$$

$$= \frac{1}{2\Delta r_i}(\vec{Y}_{1,k} - \vec{Y}_{2,k}) + \frac{1}{2\Delta r_i}\vec{Y}_{*r} \qquad (25b)$$

$$\left.\frac{\partial \vec{Y}}{\partial \zeta}\right|_* = \frac{1}{2\Delta \zeta_k}\left[(\vec{Y}_{1,k+1} - \vec{Y}_{1,k}) + (\vec{Y}_{2,k+1} - \vec{Y}_{2,k})\right]$$

$$= \frac{1}{2\Delta \zeta_k}(\vec{Y}_{1,k+1} - \vec{Y}_{1,k}) + \frac{1}{2\Delta \zeta_k}\vec{Y}_{*\zeta} \qquad (25c)$$

$$\left.\frac{\partial \vec{Y}}{\partial t}\right|_* = \frac{1}{4\Delta t_j}\left[(\vec{Y}_{1,k} - \vec{Y}_{4,k}) + (\vec{Y}_{1,k+1} - \vec{Y}_{4,k+1})\right.$$

$$\left. + (\vec{Y}_{3,k} - \vec{Y}_{2,k}) + (\vec{Y}_{3,k+1} - \vec{Y}_{3,k})\right]$$

$$= \frac{1}{4\Delta t_j}(\vec{Y}_{1,k} - \vec{Y}_{4,k}) + \frac{1}{4\Delta t_j}\vec{Y}_{*t} \qquad (25d)$$

By substituting the formulas (25) into equation (20) and evaluating the matrices $\tilde{A}$, $\tilde{B}$ and $\tilde{C}$ and the vector $\vec{T}$ at the point * one obtains equation (23) with terms (24) and $\delta = 2$ and with the modification that Δt_j is replaced by $2\Delta t_j$ in all the terms of (24).

At any level k at which the finite difference equation (23) is evaluated either the box or the zig-zag box is set up depending on the sign of v. The resulting algebraic equations for solving the unknowns $\vec{Y}_{1,k} = \vec{Y}_{i+1,j+1,k}$ for $k=1,\ldots,K_T$ will satisfy the zone of influence and dependence criteria.

It should also be noted that this whole method can be used with only a trivial change in indexing to march in the negative t direction for decreasing values of j if the main stream velocity is in the +r and -t direction. In this case the indices l=3,4 simply change to (i,j+2) and (i+1,j+2) respectively for the box method and (i,j) and (i+1,j+2) for the zig-zag box method.

Finally, it should be mentioned that the box method can be used as a set up for calculating the symmetry plane boundary layers along either r=0 or t=0 by simply setting points 1 and 2 the same and points 3 and 4 the same (t=0 symmetry plane) or points 1 and 4 the same and points 2 and 3 the same (r=0 symmetry plane).

Section 3

STARTING A THREE DIMENSIONAL BOUNDARY LAYER CALCULATION

All boundary layers begin at a nodal point of attachment and radiate outwards from this point like a polar coordinate system. The flow at the stagnation point can be calculated in isolation of the rest of the flow as shown in Part I of this report. Indeed, nodal stagnation point flow serves as the initial conditions of the rest of the boundary layer.

Because the boundary layer radiates outwards from a nodal stagnation point, it is natural to calculate the full boundary layer in a polar surface coordinate system whose pole coincides with the stagnation point. In most cases, in particular the present case, there is at least one plane of symmetry passing through this stagnation point and it is convenient to measure the azimuthal angle θ from this plane of symmetry. The stagnation point boundary layer calculation produces two components of velocity. One component radially outwards in the direction of the symmetry plane and the other component radially outwards in the direction perpendicular to the symmetry plane. From these two components the velocity in any radial direction can be obtained by simple rotation.

The next step in the calculation is to advance the solution along the symmetry plane $\theta=0$ (say the upper side) or $\theta=\pi$ (the lower side). These calculations can also be made independently of the rest of the boundary layer. Once one these calculations have been made the boundary layer is known on at least two boundaries of the strip. These boundaries are $r=0$, $\theta\varepsilon[0,\pi]$; $r>0$, $\theta=0$ or $r>0$, $\theta=\pi$. Thus, the rest of the boundary layer can be calculated by advancing a step Δr from the last radial position and marching, or sweeping in θ for constant r, from one boundary, say $\theta=0$, to the other, say $\theta=\pi$ (or vice-versa). This scheme is illustrated below.

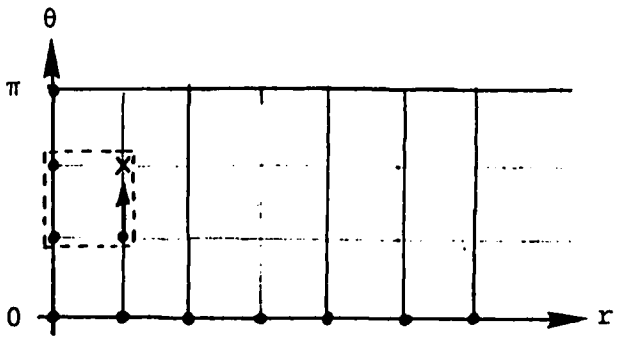

In this schematic the dots are points at which the boundary layer is known. The arrow indicates the direction of computational advance for fixed values of r and the point x is the current position at which the boundary layer is to be calculated. Note that in the box scheme, indicated by the dotted box, the three known points are used to calculate the unknown point. There is just the right amount of data to make the system determinate.

If the calculation method cannot be arranged so that rectangular groups of four points contain only one unknown then the box method, or the zig-zag box, by itself cannot be applied because there would be more unknowns than equations.

Consider then the formulation of the boundary layer problem in a locally rectangular coordinate system near the front stagnation point. Suppose this system is called (x,y) and that x=0 (y coordinate) is the plane of symmetry. Then calculation of the stagnation point and plane of symmetry yields the situation depicted below.

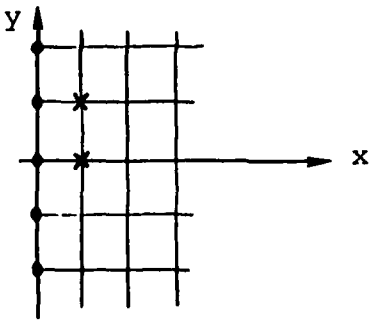

By advancing Δx to the next station it can be seen that at the first step the box will have two points of unknowns and is thus indeterminate. Thus, a special procedure needs to be used to get the first starting point when advancing to station $x+\Delta x$. It will be shown in the next section that for wing-like bodies it is necessary to use a locally rectangular system rather a polar system to integrate the three dimensional boundary layer equations.

Section 4

CALCULATION OF THE FLOW OVER AN OBLATE SPHEROID-POLAR COORDINATE

4.1 COORDINATE SYSTEMS

The most convenient coordinate system for calculating thee dimensional boundary layers is a polar system with the pole at the front stagnation point. For the oblate spheroid a polar system with poles at $z=\pm 1$ is the following:

$$\vec{R} = \sqrt{1-z^2}\ (\tau\cos\theta\vec{i} + \sin\theta\vec{j}) + z\vec{k} \qquad (26)$$

In this coordinate system the curves of z=constant are ellipses in planes of constant z and the curves of θ=constant are ellipses in meridianal planes through the z-axis. This coordinate system is nonorthogonal. However, for a sphere, $\tau=1$, the system is orthogonal. The curves $\theta=0$ and π are the intersections of the body with the x,z plane. The curves $\theta=\pm\pi/2$ are the intersections of the body with the y,z plane. The curves $\theta=0$ and π are symmetry lines of attachment in general. The curves $\theta=\pm\pi/2$ are symmetry lines of attachment for zero angle of attack.

The metric coefficients and unit vectors associated with the (z, θ) coordinates system are easily computed. These quantities are the following:

$$\vec{e}_z = (-\tau z\cos\theta\vec{i} - z\sin\theta\vec{j} + \sqrt{1-z^2}\vec{k})/g_z$$

$$\vec{e}_\theta = (-\tau\sin\theta\vec{i} + \cos\theta\vec{j})/g_\theta$$

$$g_z = \sqrt{1-z^2\lambda^2\cos\theta}$$

$$g_\theta = \sqrt{\tau^2 + \lambda^2\cos^2\theta}$$

$$h_z = g_z/\sqrt{1-z^2}$$

$$h_\theta = \sqrt{1-z^2}\ g_\theta$$

$$g = -z\lambda^2\sin\theta\cos\theta$$

where h_z, h_θ, and g are the metric coefficients.

The potential flow in terms of these coordinates are easily obtained by noting that from equations (1) and (26) the relation between the (μ,ω) and (z,θ) coordinates is

$$\left.\begin{aligned} \mu &= \sqrt{1-z^2}\,\cos\theta \\ \cos\omega &= z/\sqrt{\sin^2\theta + z^2\cos^2\theta} \end{aligned}\right\} \qquad (27)$$

It must be noted that the velocity components from the (μ,ω) system must be transformed to the (z,θ) system by equations (11).

When the spheroid is at an angle of attack the front stagnation point moves off the pole $(\mu=0,\ \omega=0) = (z=-1,\ \theta=0)$ to the point $(\mu=\mu_o,\ \omega=0) = (z=z_o,\ \theta=0)$. The value μ_o is given by

$$\mu_o = \alpha/\sqrt{1+\alpha^2} \qquad (28)$$

from Eq. (3). It is possible to form a locally (distorted) polar coordinate system about the stagnation point. This can be done by starting with a locally rectangular system about the front stagnation point. The original elliptic coordinates (μ,ω) serve this purpose.

The following embedded circle transformation with pole at $(\mu_o,0)$ can be used at the front stagnation point.

$$\left.\begin{aligned} \mu &= \mu_o + (n^2-1)\mu_o r(r+\cos\phi)\Delta \\ \sin\omega &= (n^2-1)\mu_o r \sin\phi\Delta \end{aligned}\right\} \qquad (29)$$

where $\Delta = (1+2r\cos\phi+r^2)^{-1}$

and $n>1$. The value of $n=2$ is appropriate here. A schematic diagram of this coordinate system is shown in Figure 3. Note that for $r<<1$ the system reduces to the simple polar form

$$\left.\begin{aligned} \mu &= \mu_o + \mu_o(n^2-1)r\cos\phi \\ \sin\omega &= \mu_o(n^2-1)r\cos\phi \end{aligned}\right\} \qquad (30)$$

Also, for $r = \frac{1}{n}$ equations (29) reduce to a circle in the (μ,ω) plane given by

$$\left.\begin{aligned} \mu &= n\mu_o\cos\eta \\ \sin\omega &= n\mu_o\sin\eta \end{aligned}\right\} \qquad (31)$$

where $\tan\frac{1}{2}\eta = \frac{n-1}{n+1}\tan\frac{1}{2}\phi$

This coordinate system may not be used for values of $r>1/n$. But note that for $r=1/n$ the outer boundary of this system has already encompassed the nose of the body ($z=-1$). Then once the calculation has reached the radius $r=1/n$, a switch can be made to the system defined by equation (26) which has its pole at $z=-1$. The boundary layer data in the (r,ϕ) system only needs to be interpolated onto the appropriate (z,θ) points. From this point on, there are no problems due to occurence of coordinate system poles on the rest of the body. The pole at $z=1$ is not a problem because the boundary layer separates ahead of this point.

The details of implementing these coordinate system need not be dealt with here. It is fairly obvious, based on the discussion in Section 2, what calculations need to be done. These algebraic manipulations are straight foreward but tedious.

4.2 COMPUTATIONAL RESULTS ON THE SYMMETRY PLANES

As a first test of the computational method (after successful basic checkout on a sphere) the boundary layer on the horizontal symmetry plane (the z,y plane, $x=0$) of a 25% thick ($\tau=0.25$) oblate spheroid was calculated. Here the (z,θ) system of equation (26) was used. The symmetry plane considered is thus the $\theta=0$ curve.

Figure 4 shows a plot of the displacement thickness and effective blowing velocity on the leading edge of this oblate spheroid. What is interesting to note is that the displacement thickness δ_* actually decreases in the neighborhood of separation z=0.233 (near $\omega=1.15\pi/2$). Also the effective blowing velocity w_* (a quantity of importance for viscous/inviscid interaction calculations) decreases towards separation. In two dimensional boundary layers these quantities diverge to infinity near separation. However, in this three dimensional case there is also a cross flow, as depicted in Figure 5 on a greatly expanded scale. This cross flow removes fluid from the side of an elementary volume of fluid. Hence the growth of the height of this volume is reduced. The cross flow shown in Figure 5 is at the station $\omega=107.4^{o}$, just slightly ahead of separation. It must be noted here that the separation that is being referred to is of the component of the flow in the z direction around the leading edge. The value of $\omega=107.4^{o}$ is just around the tip towards the trailing edge side. Figure 5 is a great circle cut through the x-axis.

Figure 6 shows two cross flow velocity profiles. One at station $\omega=101.5^{o}$ and the other at $\omega=107.4^{o}$. The first is just slightly beyond the the $\omega=90^{o}$ tip of the disk where cross flow reversal begins. These reversed flow cross flow

profiles clearly show the concentrated vortex that forms in the boundary layer at the tip of the disk. Because of the symmetry of the disk at zero angle of attack these vortices are symmetrically disposed over the top and bottom.

The first question that comes to mind when considering nonzero values of angle of attack, α_*, is whether one of the vortices disappears. This is expected since it seems that angle of attack would thicken one of these vortices and thin the other. That is, the pressure on the lower (windward) side of the disk would become more favorable and over the upper (leeward) side the pressure gradients are more unfavorable, i.e., tend to promote separation.

In order to investigate these questions, the horizontal plane of symmetry calculation must be abandoned and a full three-dimensional calculation must be performed. However, in the full three dimensional case of the disk at a nonzero value of the angle of attack α_*, the vertical plane, (z,x), is a plane of symmetry. The full three-dimensional calculation must begin at this plane of symmetry and march outwards towards the tip of the disk at $y=\pm 1$. Thus, since the vertical plane of symmetry is required for the 3D boundary layer calculation, it is instructive to consider it here in isolation.

Figure 7 shows the distribution of the chordwise component (z-component for $\theta=0$ and π) of skin friction coefficient C_{fz} and the cross flow component (in the direction of $\theta>0$, but at $\theta=0$) $C_{f\theta}$ of skin friction coefficient. The windward side is the bottom (pressure) side of the disk on which nothing of great interest occurs until practically at the trailing edge. Over the leeward (suction) side of the disk it is interesting to note how the cross flow reverses direction z. Note that $|C_{f\theta}|$ is plotted here! However, the streamwise flow (z-component) of the flow is not even close to separating. Thus, even over the flat upper side of the disk, three dimensionality of the flow is very prominent and there will be embedded longitudinal vortices close to the longitudinal centerplane of the disk.

The aim now is to calculate the complete three dimensional flow field and this work is described in the next section.

4.3 COMPUTATIONAL RESULTS OF THE FULL 3D BOUNDARY LAYER

Before attempting to calculate the three-dimensional boundary layer at an angle of attack it was thought desirable to calculate it at zero angle of attack first. Thus we consider the boundary layer on an oblate spheroid at zero angle of attack in edgewise flow. The (x,θ)

coordinate system of Eq. (26) was used since at zero angle of attack the front stagnation point lies right at the pole of this system.

When calculating the boundary layer on the spheroid at a nonzero angle of attack, α_*, one has to integrate outwards from the $\theta=0$ symmetry plane, the vertical, (x,z), plane.

It was found that for spheroids of thickness $\tau>0.6$ the boundary layer could be successfully calculated in this way. The results will not be shown because they are relatively small perturbations of the sphere boundary layer. However, for $\tau<0.6$ the calculation advancing away from the vertical symmetry plane becomes unstable and cannot proceed around the body.

Figure 8 illustrates this phenomena. The z-component skin friction coefficient, C_{fz}, is plotted versus the azimuthal coordinate angle θ. Note: the "z-component" does not mean a component parallel to the z-axis. When referring to the boundary layer z is a parametric surface coordinate that runs roughly in the same direction as the z-axis. The points on the surface corresponding to the z parameter are in a one-to-one correspondence with points on

the z-axis that have the same value of z. In Figure 9 the small circles are computed values of C_{fz} when the calculation method advances from the vertical symmetry plane towards the tip of the disk ($\theta=0$ to $\theta=\pi/2$). The solid curve is the C_{fz} distribution at the same station z (cross-section) calculated by advancing from the horizontal symmetry plane inwards towards the vertical symmetry plane of the disk. It can be seen that there is a large discrepancy in these predictions of C_{fz}. The calculation that advanced from the vertical plane of symmetry broke down shortly after station z=0.25. The calculation that advanced from the horizontal plane of symmetry continued to separation that started at about z=0.25 and $\theta=\pi/2$ (i.e., just beyond the maximum diameter of the body).

The most important aspect of this calculation is that the method of advancing the calculation azimuthally around the stagnation point starting from the vertical symmetry plane will not work for disks of thickness τ less than about 0.6. The reason for this is that in a polar coordinate system, with pole through the front stagnation point, the boundary layer is advanced downstream a distance Δr and then swept azimuthally around the body either from the leeward side around the edge and then towards the windward symmetry plane or vice-versa. In either case, this azimuthal sweep will have to advance, at some point, towards the

edge of the disk. In this part of the sweep, the external inviscid flow component in the azimuthal direction points against the sweeping direction of the calculation method. Even the zig-zag box cannot manage such a strong reversed cross flow. The zig-zag box method can only cope with weak reversed cross flow deep in the boundary layer. The method cannot march against the external inviscid flow.

Some calculations were made by advancing from the vertical symmetry plane around the azimuth for a disk at an angle of attack using the coordinates defined by (29). Again for very thick disks, $\tau>0.6$, the boundary layer could be calculated successfully, but not for thin disks $\tau<0.6$. We are mainly interested here in very thin disks, $\tau<0.1$, simulating propeller blades. Thus a new method for calculating the 3D boundary layer had to be developed.

If a surface rectangular coordinate system is used in which one set of coordinate lines run nearly longitudinally down the body (from z=-1 to z=1) and the other set of lines run outwards from the vertical symmetry plane towards the tip, then these coordinates are more nearly aligned with the external flow over the body. In terms of high aspect ratio wings, one might say the coordinate lines are chordwise and spanwise. A calculation method based on such a system is described in the next section.

Section 5

CALCULATION OF THE FLOW OVER AN OBLATE SPHEROID-SURFACE RECTANGULAR COORDINATES

5.1 THE COORDINATE SYSTEM

The coordinate system that is suitable for thin bodies in nearly edgewise flow, such as wings and blades, is one with coordinates that are roughly chordwise and spanwise. Such surface coordinates are roughly rectangular except for the stretching required to fit them over a curved surface. A rectangular system does not have any poles and thus in the neighborhood of the origin (or any other point) the metric coefficients are approximately constant. In a polar coordinate system one metric coefficient is always a function of a coordinate to first order.

A suitable coordinate system to deal with the disk boundary layer is the (r,t) system which gives the following disk representation:

$$\vec{R}(r,t) = \sqrt{1-r^2}(\tau\sin(t-t_o)\vec{i} + \cos(t-t_o)\vec{k}) + r\vec{j} \quad (32)$$

where t_o corresponds to the value of t of the front stagnation point μ_o. By comparing equations (1) and (32), it can be seen that

$$\mu = \sqrt{1-r^2}\,\sin(t-t_o)$$

and (33)

$$\sin\omega = r/\sqrt{\cos^2(t-t_o)+r^2\sin^2(t-t_o)} \quad .$$

Thus the point r=0, $t=t_o$ of the front stagnation point corresponds to $\mu=\mu_o$, $\omega=0$ so that

$$t_o = -\sin^{-1}(\mu_o) \quad . \tag{34}$$

The coordinate system (r,t) is nonorthogonal with metric coefficients

$$h_r = \sqrt{1-\lambda^2 r^2\sin^2(t-t_o)}/\sqrt{1-r^2}$$

$$h_t v = \sqrt{1-\lambda^2\cos^2(t-t_o)}/\sqrt{1-r^2}$$

$$g = \lambda^2 r\sin(t-t_o)\cos(t-t_o) \quad .$$

The unit vectors $\vec{e}_r$ and $\vec{e}_t$ are easily computed using equation (32) and thus the potential flow velocity

$$\vec{V} = U_r\,\vec{e}_r + U_t\,\vec{e}_t$$

is also easily computed with the help of equations (3) and (11).

It is to be noted that the surface coordinate (r,t) has the configuration near the front stagnation point depicted schematically below:

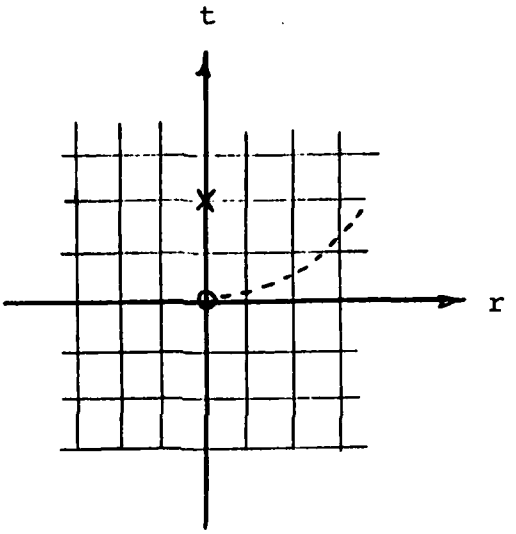

Schematic of the (r,t) coordinate system.

In this schematic 0 is the front stagnation point, x is the nose of the disk on its leading edge and the dashed curve is the line of attachment of the flow. The line of attachment is the curve on the body which separates the potential flow into two regions. The flow above the line of attachment has a positive t-component of velocity that goes over the top (leeward) side of the body. The flow below the line of attachment has a negative t-component of velocity

that goes under (windward) side of the body for positive values of the angle of attack α_*.

5.2 THE CALCULATION OF THE BOUNDARY LAYER

The calculation of the boundary layer in the (r,t) coordinate system of equation (32) meets with the difficulty of stepping the boundary layer from station r to r+Δr described in Section 3. The procedure is basically to calculate the stagnation point boundary layer and the vertical plane of symmetry, r=0, boundary layer for both positive and negative values of t. Once this has been done, the next step is to increment the value of r to r+Δr. At this stage one is faced with having to compute the boundary layer at the new value r+Δr without having available any r+Δr points at which the boundary layer is known. It is clear from the description of the box and zig-zag box method of Section 2.3 that these methods are not applicable until at least one point on the r+Δr line (i+1) station has the boundary layer specified.

A novel way to obtain this required data was first suggested by Schwamborn (1981). In this method the zig-zag box scheme is applied simultaneously to the first two points on the r+Δr line (i+1) shown schematically in Figure 9. A foreward zig-zag box is applied to the points (j+2,i), (j+1,i), (j+1,i+1) and (j,i+1) where the point (j+1,i+1) is

considered to be the principal unknown and the point (i+1,j) is presumed known (by a guess or prior iteration). This computational molecules is shown as the solid outline in Figure 9. A second, overlapping, zig-zag scheme, shown by the dashed outline in Figure 9, is used to determine the boundary layer at the point (i+1,j) given the known data at points (i,j), (i,j-1) and (i+1,j+1). By simultaneously iterating these two zig-zag schemes it seems that the boundary layer at the two points (i+1,j+1) and (i+1,j) could be determined. If this scheme converges then the rest of the points on the line $r+\Delta r$ can be calculated by the standard box method.

Unfortunately, we have not been able to make this method work, although Schwamborn claims that it does work. We believe the method should converge. At this stage, our inability to achieve success with the method may be due to coding errors, though very careful checks, not only by the principal investigator but also independently by another scientist has not turned up any coding errors. Thus, the method stands at an impasse and no results have been obtained for the full three-dimensional boundary layer calculation for the oblate spheroid at an angle of attack.

Section 6

CONCLUDING REMARKS

The research effort to develop computational methods for calculating propeller blade leading edge boundary layers is at the following stage.

(i) A numerical method for dealing with the 3D laminar boundary layer equations, with rotation, and in non-orthogonal surface coordinates has been developed and programmed.

(ii) The method has been set up in a a general way so that a variety of coordinate systems can be handled easily as demonstrated in Sections 4 and 5 of this report.

(iii) The method can deal successfully with non flat bodies such as ship bows and elongated bodies at zero or nonzero angles of attack, such as ovary spheroids or, more practically, submarines or torpedoes. In fact, the same basic set of algorithms and codes were used for the direct numerical integration of the attachment line boundary layer of Part I. This type of calculation has direct relevance to destroyer bows.

(iv) A new method for advancing from the stagnation point along the foreward curve of attachment near a leading edge of a flattened body such as a wing or blade was unsuccessful. The method does not seem to have any flaws and at this time it is not certain whether coding errors have prevented success in using this method.

(v) Some alternative methods to achieve success in calculating the leading edge flow might be to use an explicit backward differencing with respect to the t-coordinate or to apply the characteristic box method. Resources of the present contract have not permitted us to embark on efforts to develop these alternative methods. It is believed, that a modest further effort can resolve the problem at the attachment line and result in a very useful, and versatile three-dimensional boundary layer code.

REFERENCES

Cebeci, T., Khattab, A.A. and Stewartson, K. (1981), "Three-dimensional laminar boundary layers and the Ok of accessibility," J. Fluid Mech., 107, 57.

Cebeci, T. (1985), "Problems and opportunities with three-dimensional boundary layers" in Three-Dimensional Boundary Layers, AGARD Report No. 719, Brussels, Belgium.

Durand, W.F. (ed.) (1963), "Fluid Mechanics, Part II," Aerodynamic Theory, Dover.

Groves, N.C. (1981), "An integral prediction method for three-dimensional turbulent boundary layers on rotating blades," Propellers '81, Soc. Nav. Arch. Marine Eng., New York.

Groves, N.C. and Chang, M.S. (1985), "A differential prediction method for three-dimensional laminar and turbulent boundary layers of rotating propeller blades," DTNSRDC Report 85/058.

Schwamborn, D. (1979), "Laminane Grenzschichten in der Nähe der Anlegelinie an Flügeln und Flügelähnlichen Körpern mit Anstellung," Doctoral Thesis, RWTH Aachen.

Squire, L.C. (1955), "The three-dimensional boundary layer equations and some power series solutions," British R.&M., No. 3006.

Section 8

FIGURES

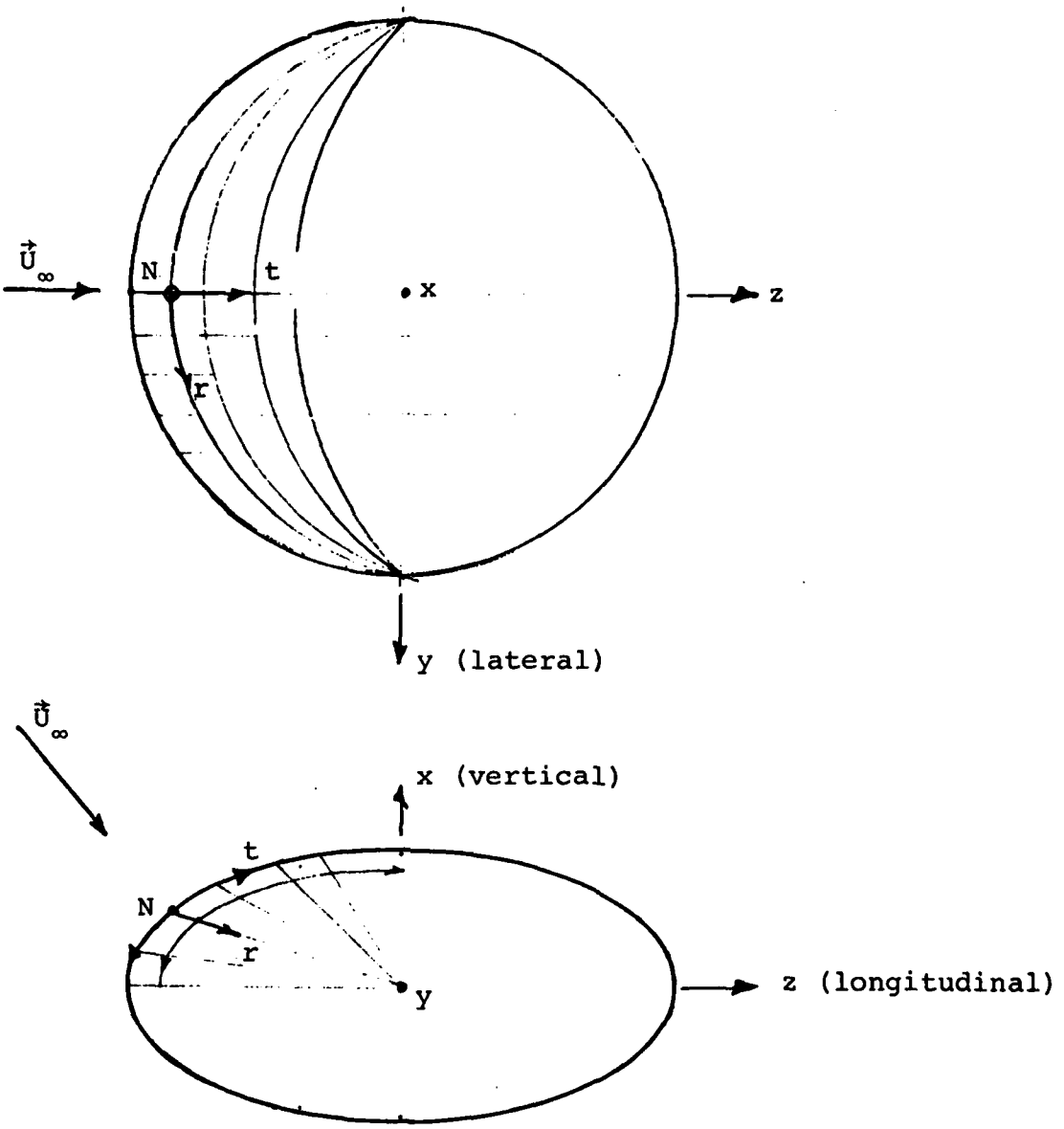

Figure 1. Edgewise flow past an oblate spheroid coordinate system schematic.

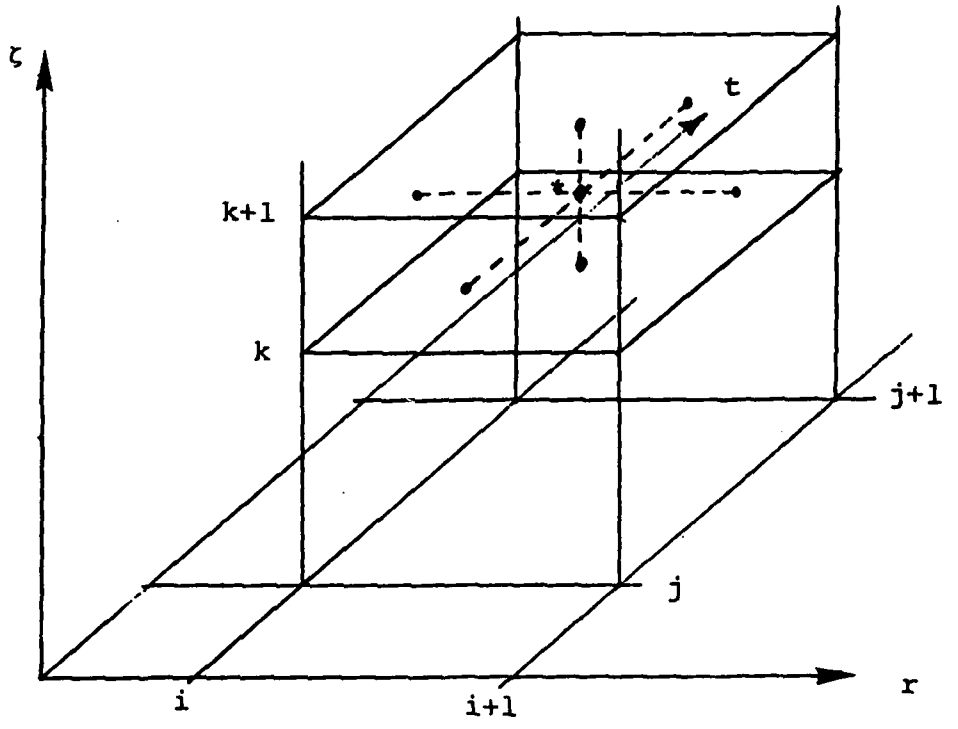

Figure 2. The box finite difference molecule.

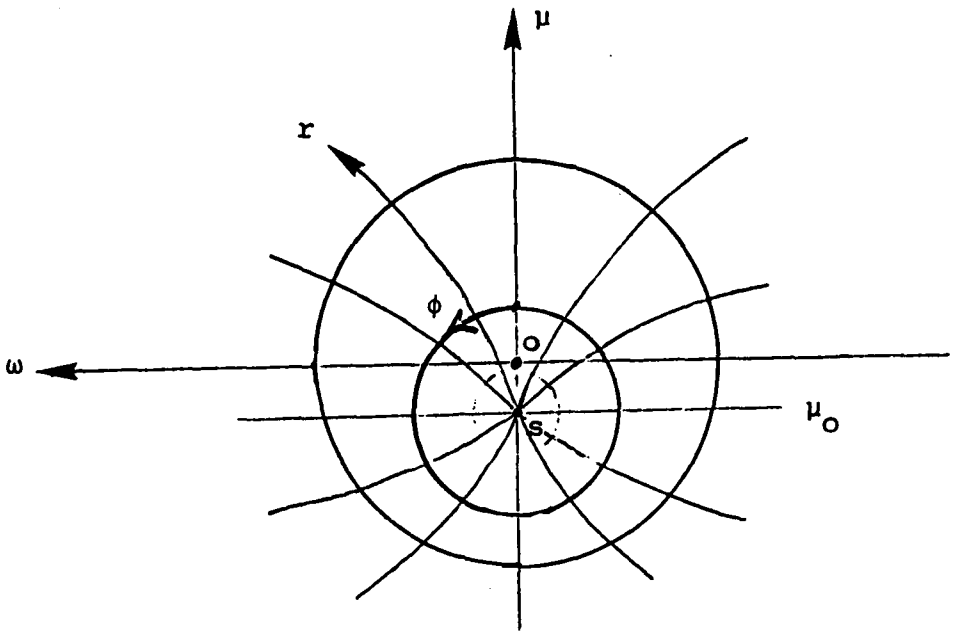

Figure 3. The embedded circle polar coordinate system. s is the stagnation point and o is the nose of the body and origin of the (μ,ω) coordinate system.

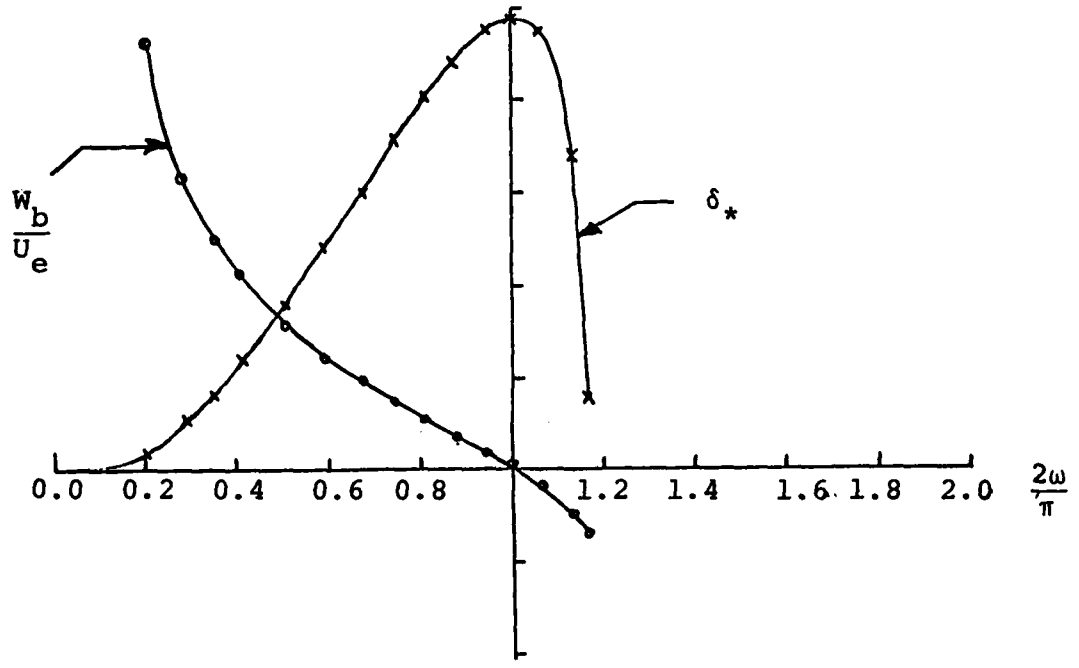

Figure 4. Effective blowing velocity, W_b, and displacement thickness δ_* for $\tau=0.25$, $\alpha_*=0$.

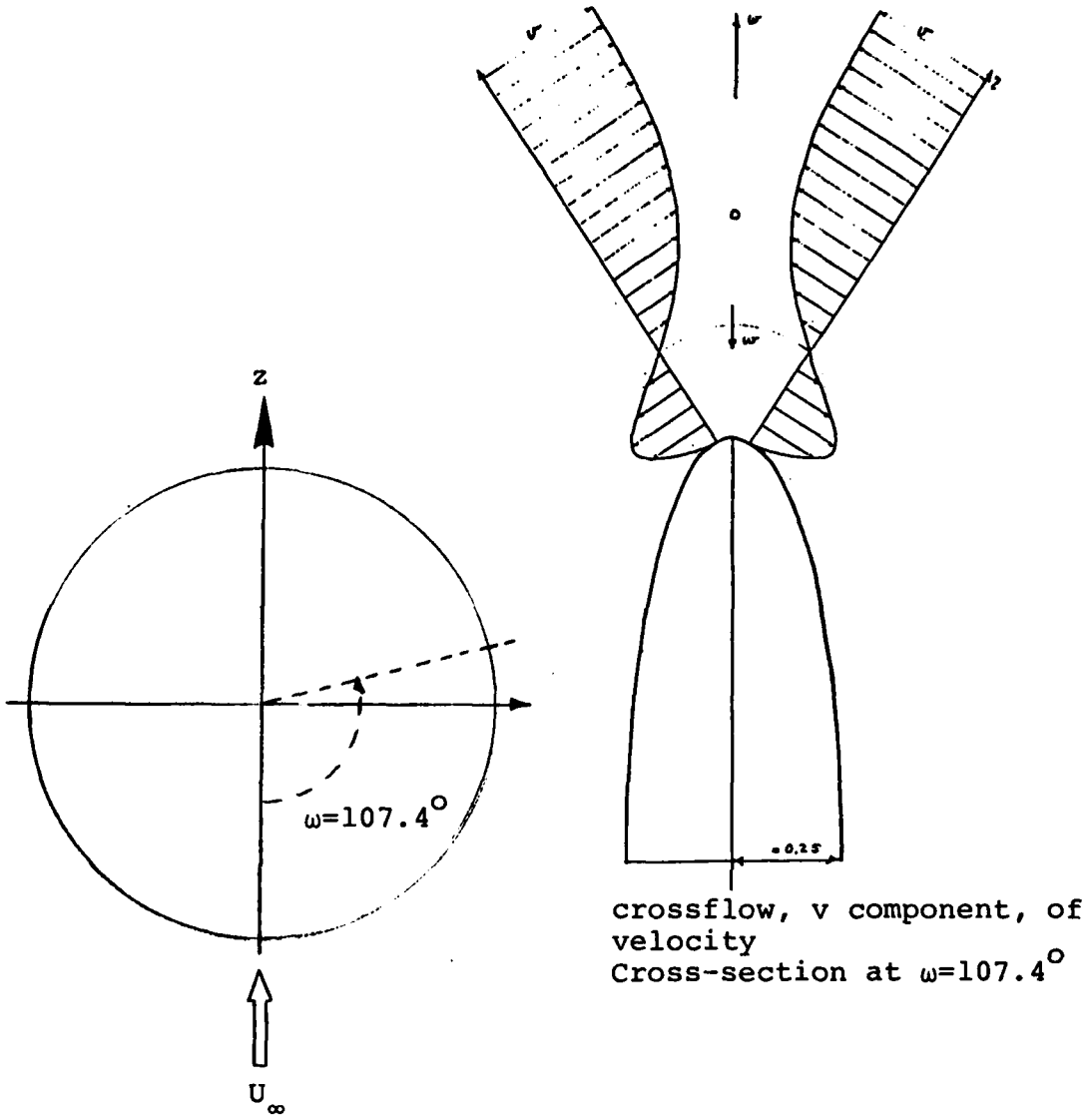

Top view of disk showing location of the cross-section in the right figure.

Figure 5. The crossflow velocity profiles (greatly expanded in scale) at the edge of the disk for $\omega=107.4^{\circ}$, just ahead of separation of the u component of velocity in the ω direction.

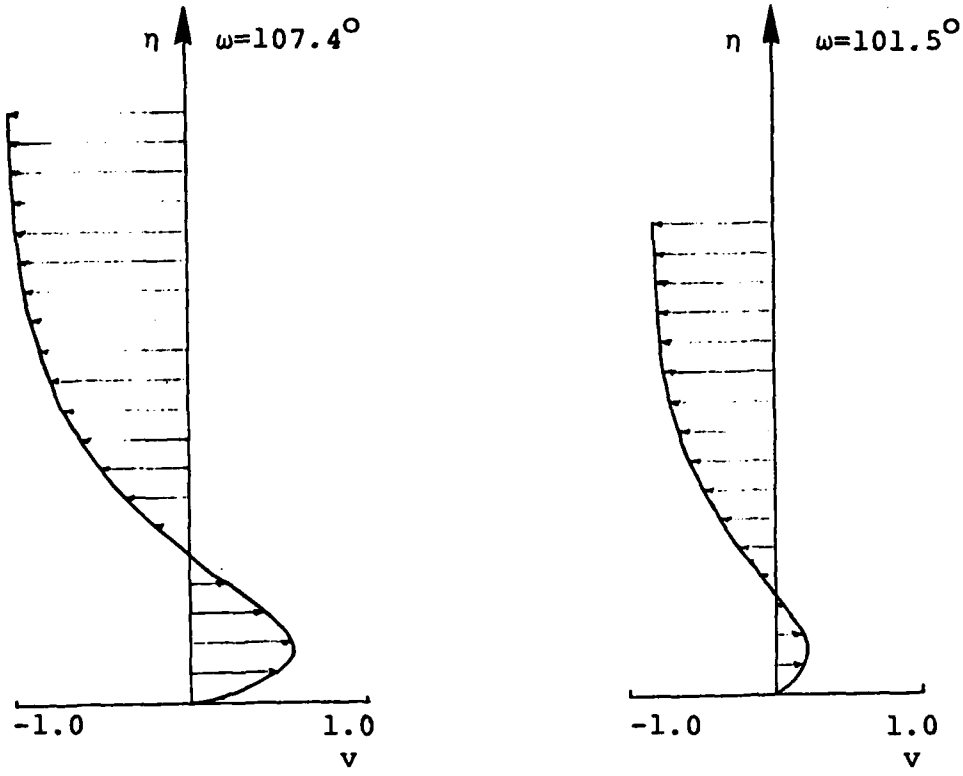

Figure 6. Cross-flow velocity profiles; τ=0.25.

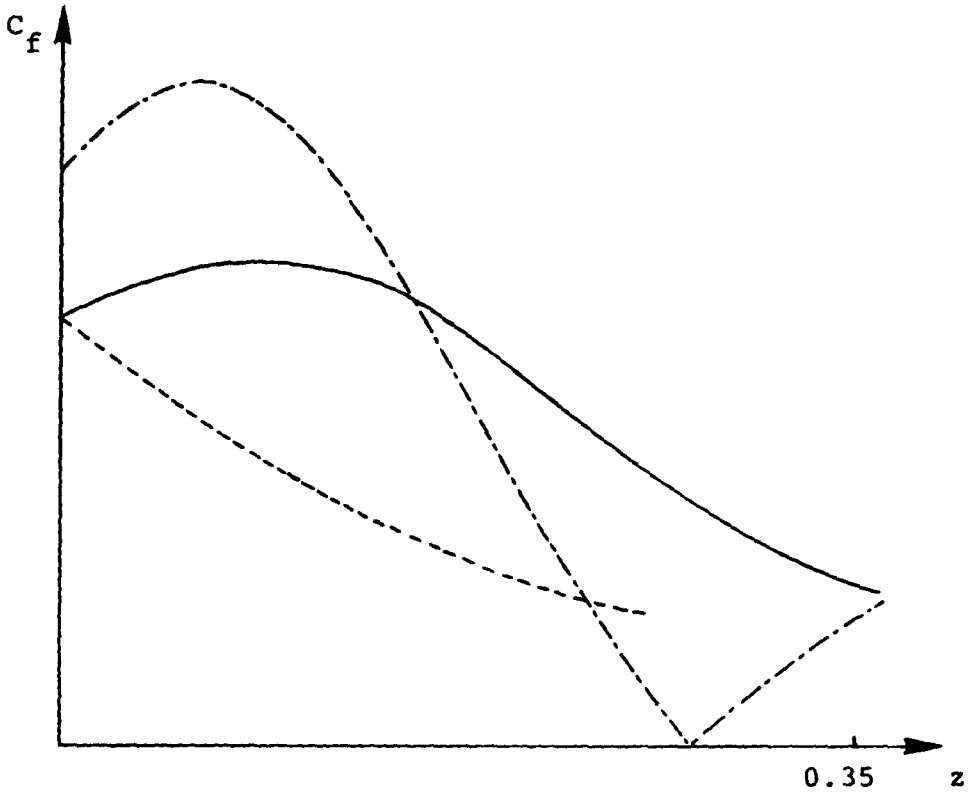

Figure 7. Skin friction coefficients C_{fz} and $C_{f\theta}$ on the vertical (x,z) symmetry plane of the disk of thickness τ=0.25 at an angle of attack α_*=0.1.

C_{fz} |-------| Windward side

C_{fz} |———| Leeward side

$|C_{f\theta}|$ |— - —| Leeward side

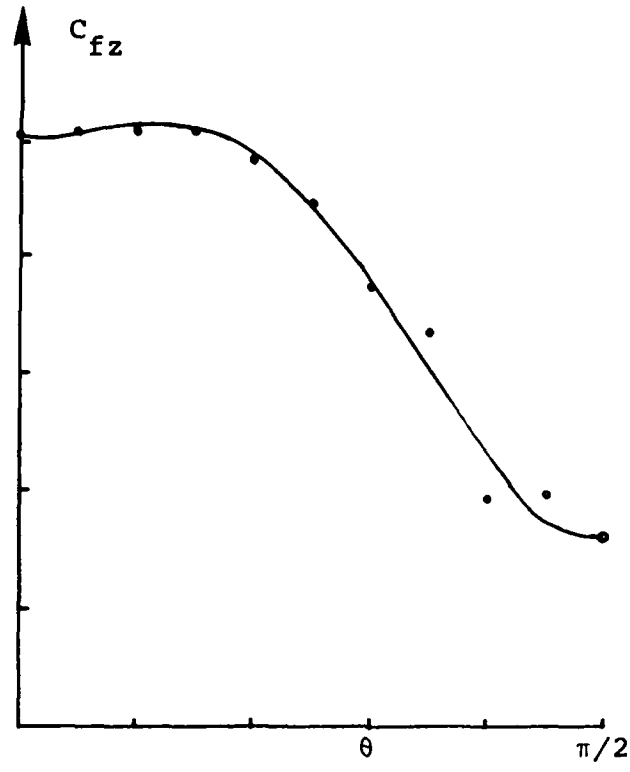

Figure 8. The azimuthal variation of the skin friction coefficient C_{fz} in the z-direction for a disk with $\tau=0.5$, $\alpha_*=0$ at station $z=-0.25$.

|——| Calculated by advancing from edge, $\theta = \frac{\pi}{2}$, to vertical symmetry plane $\theta=0$.

o o o o Calculated by advancing from vertical symmetry plane $\theta=0$ to the edge $\theta=\pi/2$.

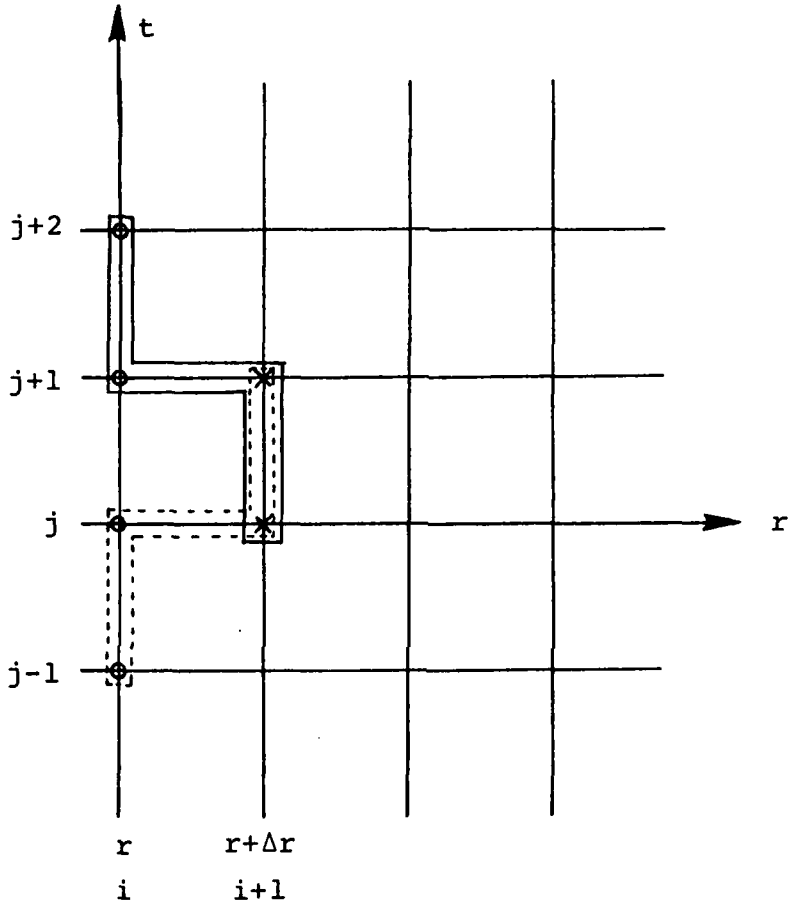

Figure 9. The computational molecule for the double zig-zag box method for the first two starting points (x) when advancing from station r to station r+Δr.

(12)

ASPECTS OF THE CALCULATION OF BOUNDARY LAYERS ON SHIPS' PROPELLERS

(FINAL REPORT)

SAIC-85/1158

SAIC™
Science Applications International Corporation
134 Holiday Court, Suite 318, Annapolis, Maryland 21401, (301) 266-0991

END

FILMED

2-86

DTIC